Supporting Information for

General pore features for one-step C_2H_4 production from C2 hydrocarbon mixture

Tao Zhang,[†a] Jian-Wei Cao,[†a] Shu-Yi Zhang,[a] He Feng,[a] Ye Li,[a] Yu Wang,[*a] Juan Chen,[a] Teng Wang,[a] Kai-Jie Chen[*a]

[a] *Key Laboratory of Special Functional and Smart Polymer Materials of Ministry of Industry and Information Technology, Xi'an Key Laboratory of Functional Organic Porous Materials, School of Chemistry and Chemical Engineering, Northwestern Polytechnical University, Xi'an, Shaanxi, 710072, China.*

[†] *These authors contributed equally to this work.*

E-mail: Yu Wang: wychem@nwpu.edu.cn; Kai-Jie Chen : ckjiscon@nwpu.edu.cn

General consideration.

The metallic salts and the ligands were purchased from Energy Chemical without further purification otherwise specifically mentioned. The tpt ligand (2,4,6-tri(4-pyridinyl)-1,3,5-triazine) was synthesized according to reported methods.[1] The PXRD patterns were recorded using Rigaku D/Max-2550VB+/PC with CuKα radiation (λ = 1.5418 Å). Thermogravimetric analysis (TGA) was conducted on 449C Jupiter analyzer under the flowing N_2. The FT-IR spectra were recorded by ThermoFisher analyzer from 400 to 4000 cm^{-1} using KBr as reference. Gas adsorption measurements were tested by Micromeritics 3Flex.

Synthesis of [$Ni_3(\mu_3$-OH)$(ina)_3(bdc)_{1.5}$] Ni-BDC-INA.

[$Ni_3(\mu_3$-OH)$(ina)_3(bdc)_{1.5}$] was synthesized according to the reported method with little modification.[2] In a 100 mL Teflon reactor, 870 mg of $Ni(NO_3)_2{\cdot}6H_2O$, 250 mg of H_2bdc and 365 mg of H_2ina (isonicotinic acid) were dissolved in the mixture of 25 mL of EtOH and 50 mL of DMF, after that, 50 μL $NH_3{\cdot}H_2O$ was added. The mixture was ultrasonically dispersed for 15 min and transferred to a stainless steel reactor. After heating at 150 ºC for 2 days, the product was harvested as green octahedral fine crystal (*ca*. 35 % based on metallic salt).

The activation of the sample was achieved by solvent exchange with acetone for 3 days followed by degassing at 130 ºC under a dynamical vacuum using a degassing station.

Synthesis of [$Co_3(\mu_3$-O)$(bdc)_3$(tpt)] CPM-173.

[$Co_3(\mu_3$-O)$(bdc)_3$(tpt)] was synthesized according to the reported method with little modification.[3] In a 100 mL Teflon reactor, 480 mg of $CoCl_2{\cdot}4H_2O$, 480 mg of H_2bdc and 250 mg of tpt were dissolved in the mixture of 25 mL of EtOH and 25 mL of DMF. The mixture was ultrasonically dispersed for 15 min and transferred to a stainless steel reactor. After heating at 130 ºC for 2 days, the product was harvested as a brick-red powder (*ca*. 30 % based on metallic salt).

The activation of the sample was achieved by solvent exchange with acetone for 3 days followed by degassing at 130 ºC under a dynamical vacuum using a degassing station.

Synthesis of UiO-66.

UiO-66 was synthesized according to a classical solvothermal method[4] and the product was harvested as a white powder (*ca*. 40 % based on metallic salt).

The activation of the sample was achieved by solvent exchange with acetone for 3 days followed by degassing at 130 ºC under a dynamical vacuum using a degassing station.

Synthesis of DMOF-1.

[$Zn_2(bdc)_2$(dabco)] (dabco = 1,4-Diazabicyclo[2.2.2]octane) was synthesized according to the reported method with little modification.[5] In a 100 mL Teflon reactor, 1.0 g of $Zn(NO_3)_2{\cdot}6H_2O$, 560 mg of H_2bdc, 187 mg of dabco were dissolved in the 50 mL of DMF and 200 μL $NH_3{\cdot}H_2O$ was added. The mixture was ultrasonically dispersed for 15 min and subsequently transferred to a stainless steel reactor and heated at 130 ºC for 3 days. After cooling down, the product was harvested as white powder (*ca*. 45 % based on metallic salt).

The activation of the sample was achieved by solvent exchange with acetone for 3 days followed by degassing at 130 ºC under a dynamical vacuum using a degassing station.

Synthesis of MOF-74-Co

[Co_2(dhtp)] (H_4dhtp = 2,5-dihydroxyterephthalate) was synthesized according to the reported method.[6] The activation of the sample was achieved by degassing at 200 ºC under a dynamical vacuum using a degassing station.

Synthesis of IISERP-MOF2

[Ni(ina)$_2$] was synthesized according to the reported method.[7, 8] The activation of the sample was achieved by degassing at 200 °C under a dynamical vacuum using a degassing station.

BET surface area calculation.

The N_2 adsorption isothermals for different samples at 77 K were fitted using the BET model as following:

$$\frac{P}{Q(P_0 - P)} = \frac{1}{Q_m C} + \frac{(C-1)P}{Q_m C P_0}$$

where Q and Q_m are gas loading at a specific pressure and saturation in single layer respectively ($cm^3\ g^{-1}$), P and P_0 are the pressure and saturated vapor pressure for nitrogen at 77 K respectively (kPa), C is a constant associated with the adsorbent. And the surface area can be calculated as following:

$$S = \frac{Q_m N_A \delta}{22400}$$

where N_A Avogadro constant ($6.023\times 10^{23}\ mol^{-1}$), δ is the section area of nitrogen molecules ($0.162\times 10^{-18}\ m^2$ for N_2).

Langmuir-Freundlich fit.

The isothermal for different gases at 298 K were fitted using the Langmuir-Freundlich model as following:

$$q = q_{sat}\frac{b_A p^n}{1 + b_A p^n}$$

where q and q_{sat} are gas loading at a specific pressure and saturation respectively, b_A is Langmuir-Freundlich constant at A site, n is Freundlich exponent and p is pressure.

Selectivity calculation.

The selectivity of equimolar C_2H_2/C_2H_4 and C_2H_6/C_2H_4 binary mixtures was calculated using ideal adsorption solution theory (IAST) method,[9] and the selectivity is defined as following:

$$S = \frac{x_A/x_B}{y_A/y_B}$$

where S is the selectivity of A towards B, x_A and x_B are the molar fractions of A and B in the adsorbent respectively, y_A and y_B are the molar fractions of A and B in the gas mixture respectively.

Table S1. A comprehensive table of gas adsorption information for indicated samples.

Material	BET surface area / $m^2\ g^{-1}$ [a]	Langmuir surface area / $m^2\ g^{-1}$ [a]	C_2H_2 uptake at 1 bar / $cm^3\ g^{-1}$ [b]	C_2H_4 uptake at 1 bar / $cm^3\ g^{-1}$ [b]	C_2H_6 uptake at 1 bar / $cm^3\ g^{-1}$ [b]	$Q_{st}(C_2H_2)$/ kJ mol^{-1} [c]	$Q_{st}(C_2H_4)$/ kJ mol^{-1} [c]	$Q_{st}(C_2H_6)$/ kJ mol^{-1} [c]	IAST selectivity for C_2H_2/C_2H_4	IAST selectivity for C_2H_6/C_2H_4	C_2H_4 productivity / mmol g^{-1} [i]	Reference
Ni-BDC-INA	849.2	NM	80.2	59.1	63.4	27.86	26.57	29.01	1.37 [d]	1.56 [d]	0.100[f]	This
CPM-173	891.3	NM	172.1	130.5	141.4	30.09	26.38	27.29	1.51 [d]	1.76 [d]	0.073 [f]	This
UiO-66	1317	NM	73.1	56.3	61.7	25.69	24.48	27.09	1.45 [d]	1.57 [d]	0.018 [f]	This
DMOF-1	1843.8	NM	101.8	72.6	102.6	24.35	20.53	20.76	1.35 [d]	1.51 [d]	0.093 [f]	This
NPU-1	1396	1557	114.2	94.1	100.8	27.88	23.95	29.1	1.4 [d]	1.32 [d]	0.129 [f]	10
TJT-100	890	1077	127.7	98.1	105.4	31	25	29	1.8[e]	1.2 [e]	0.69[g]	11
Azole-Th-1	983	NM	79.5	80.7	100.2	25.4	26.1	28.6	NM	1.46 [d]	1.34 [h]	12
ZJNU-115	1291	1404	106	84	94.2	29.2	27.7	28.2	2.05 [e]	1.56 [d]	NM	13
MIL-125	1435	NM	108.192	89.152	157.92	17.6	17	23.6	2.32 [e]	1.43 [d]	NM	14
NH2-MIL-125	1180	NM	105.1	98.8	175.2	33	23	24.8	3.75 [e]	1.18[d]	NM	14
MUV-11	180	NM	41	38.5	89.2	20.3	23.5	25	6.92 [e]	1.53 [d]	NM	14
ZSTU-2	862	NM	61.2	52.6	69.7	23.5	32	33.5	2.36 [e]	1.62 [d]	NM	14
UPC-612	2016	NM	67.447	62.581	80.11	23.94	16.94	22.39	1.06 [d]	1.38 [d]	0.47 [f]	15
UPC-613	853	NM	63.477	51.723	57.171	30.38	28.51	31.83	1.43 [d]	1.50 [d]	0.34 [f]	15
NUM-9a	330	371	52.8	52.3	55.55	35.79	32.32	35.75	1.50 [d]	1.61[d]	NM	16
Zn-atz-oba	710.7	783.1	62.05	45.47	45.92	27.49	27.07	30.05	1.27[d]	1.43[d]	NM	17
ZJNU-7	1180	1303	112.8	85.2	92.5	34.1	29.3	29.7	1.77[e]	1.56[d]	NM	18
UiO-77-$(NH_2)_2$	2815	NM	132.2	96.8	119.2	27.4	24.5	26.5	2.1[e]	1.7[d]	0.55	19

NM: not mentioned; [a] calculated from the N_2 adsorption data at 77 K;[b] at 298 K; [c] at low loading; [d] 50:50 gas mixture at 298 K and 1 bar;.[e] 1:99 gas mixture at 298 K and 1 bar; [f.] 1/1/1 ($C_2H_2/C_2H_4/C_2H_6$) ternary gas mixture; [g.] 0.5/99/0.5 ($C_2H_2/C_2H_4/C_2H_6$) ternary gas mixture; [h.] 1/9/90 ($C_2H_2/C_2H_4/C_2H_6$) ternary gas mixture; [i] The productivity was calculated using the equation:$p = \frac{F y_{C_2H_4} \int_{t_1}^{t_2} \frac{C(t)}{C_0} dt}{V_m}$, where p is productivity in mmol g^{-1}, t_1 is the C_2H_4 breaktime in min g^{-1}, t_2 is the breakthrough time of other gas, F is the inlet gas volume flow rate, y_{C2H4} is the volume fractionof C_2H_4 in mixed gas, C(t) and C_0 are the C_2H_4 concentration in the outlet and inlet gas, V_m is molar volume of gas.

Isosteric heat calculation.

The isosteric heat (Q_{st}) of gas adsorption was obtained from the isothermals of specific gas at 273 and 298 K. The data were fitted using the virial-type equation as follows,[20] where P is pressure in kPa, N is the adsorbed amount in mmol g^{-1}, T is temperature in K, R is the universal gas constant, a_i and b_j are the virial coefficients, in this study, i = 0, 1, 2, 3, 4, 5 and j = 0, 1, 2.

$$Q_{st} = -R\sum_{i=0}^{5} a_i N^i$$

$$\ln P = \ln N + \frac{1}{T}\sum_{i=0}^{m} a_i N^i + \sum_{j=0}^{n} b_j N^j$$

Breakthrough experiments

The breakthrough experiments were conducted using a homemade facility. Firstly, the powder samples were packed into a column tightly and connected into the facility. The breakthrough experiments for all four samples were tested in stainless steel tubes with an inner diameter of 5 mm. Then the column was heated at 353 K under blowing He gas with flow rate of 20 cm^3 min^{-1} until the outlet gas exhibiting no solvent signals. After activating, the equimolar gas mixture of C_2H_2, C_2H_4 and C_2H_6 with total pressure of 100 kPa was allowed to pass through the column from one side. And a gas chromatography analyzer (TCD Thermal Conductivity Detector, detection limit 0.1 ppm) was connected to the other side of the column to detect the content of outlet gas. The C/C_0 vs time plots were generated by the following equation:

$$\frac{C}{C_0} = \frac{S}{S_{eq}}$$

where S is the integral area of a gas content at time t; S_{eq} is the integral area of a gas content when equilibrium.

Table S2. The comprehensive breakthrough experimental information for indicated samples.

Material	Sample mass / g	Breakthrough time of C_2H_2 / min ($C/C_0 \geq 0.01$)	Breakthrough time of C_2H_4 / min ($C/C_0 \geq 0.01$)	Breakthrough time of C_2H_6 / min ($C/C_0 \geq 0.01$)
Ni-BDC-INA	2.60	123	118	134
CPM-173	2.30	106	92	95
UiO-66	1.80	88	78	80
DMOF-1	3.50	190	182	196
MOF-74-Co	1.68	346	252	193
IISERP-MOF2	1.98	81	80	84

Grand Canonical Monte Carlo (GCMC) simulations.

The Grand Canonical Monte Carlo (GCMC) simulations were performed to reveal the host-guest interactions using the Sorption module in Material Studio software package**.** To build the simulation boxes, supercells of 1 ×1 ×1 for **Ni-BDC-INA**, 2 ×2 ×2 for **CPM-173**, 1 ×1 ×1 for **UiO-66**, and 2 ×2 ×2 for **DMOF-1** were used after making $P1$. All the frameworks and gas molecules were both treated as rigid bodies and the Q_{eq} fitted charge and the ESP charge were

assigned to the hosts and guests respectively. The loading steps, equilibration steps, and production steps were all set to 2.0 × 10^7. The Metropolis method was applied during the simulation.[21] All the host-guest interaction behavior was described using Universal force field (UFF).[22] The cut-off radius used for the Lennard–Jones interactions is 18.5 Å.

Table S3. Calculated interaction energy for selected MOFs using GCMC simulation.

Material	C_2H_2/ kJ mol^{-1}	C_2H_4/ kJ mol^{-1}	C_2H_6/ kJ mol^{-1}
Ni-BDC-INA	34.80	27.87	40.32
CPM-173	30.65	24.53	36.93
UiO-66	31.88	25.22	36.85
DMOF-1	24.95	23.79	26.06

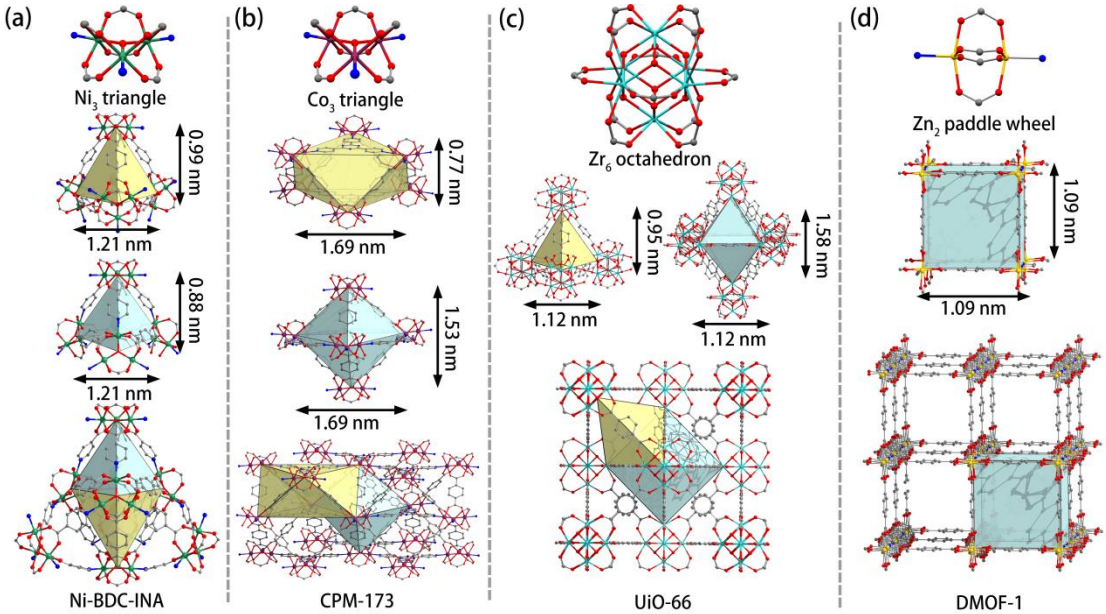

Figure S1. The polyhedral cages and structural informations for (a) **Ni-BDC-INA**; (b) **CPM-173**; (c) **UiO-66** and (d) **DMOF-1**. Colour code: C, grey; O, red; N, blue; Ni, green; Co, violet; Zr, light blue; Zn, yellow.

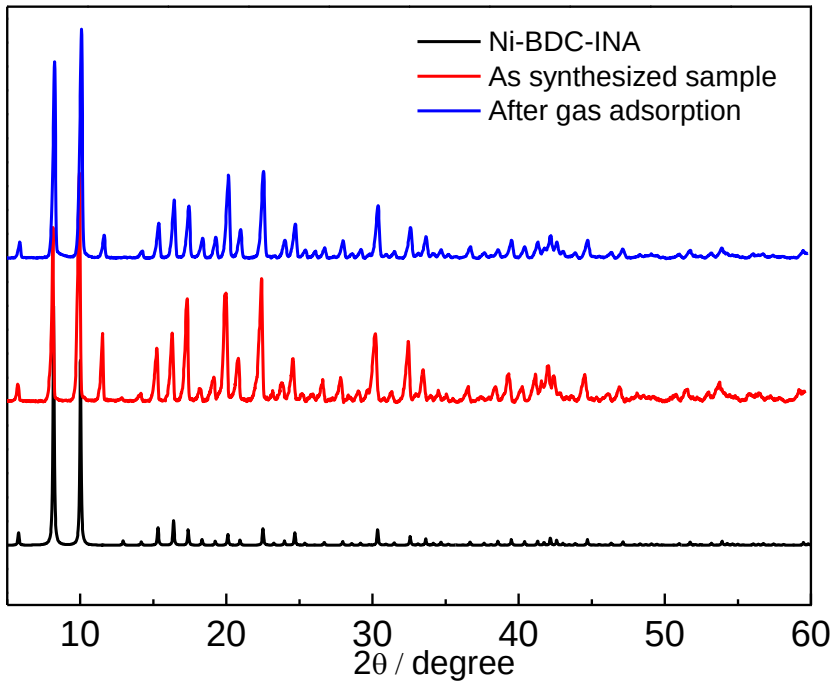

Figure S2. PXRD patterns of **Ni-BDC-INA**.

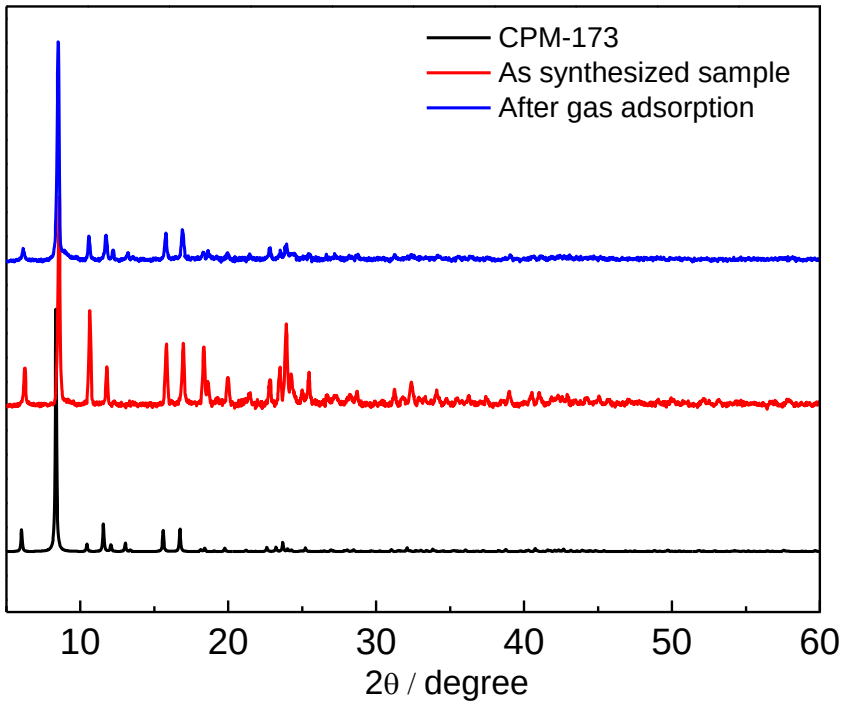

Figure S3. PXRD patterns of **CPM-173**.

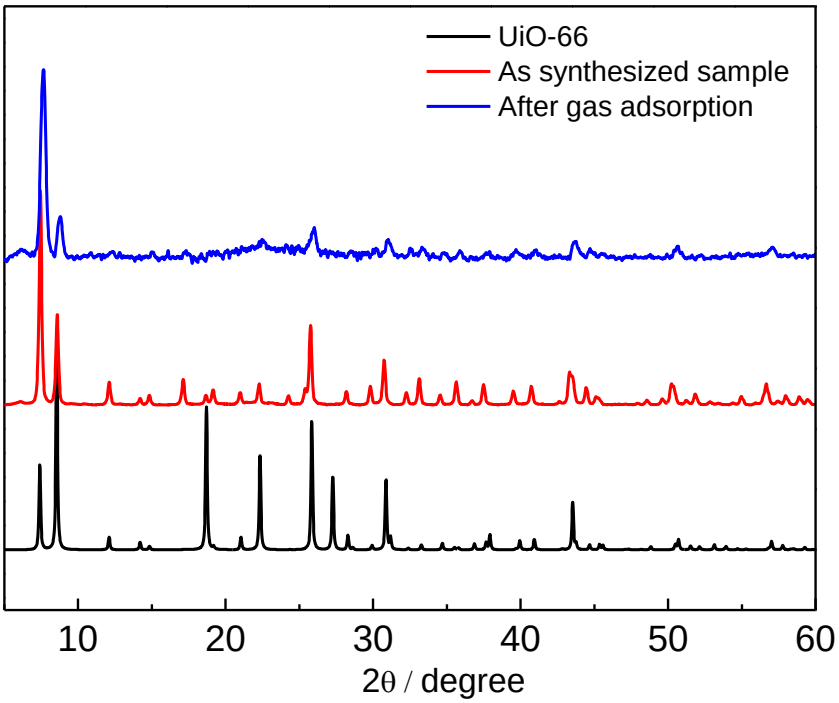

Figure S4. PXRD patterns of **UiO-66**.

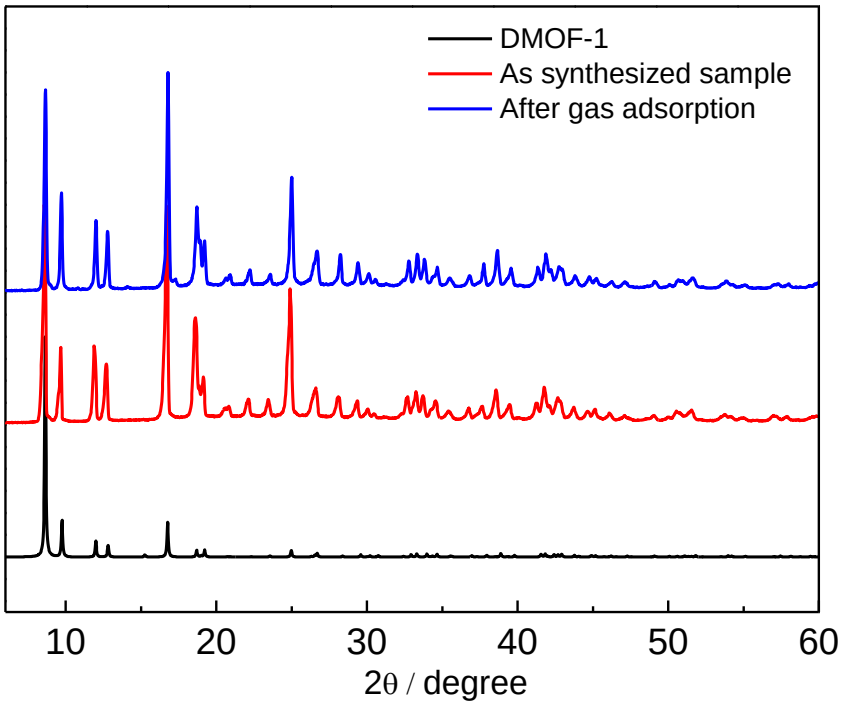

Figure S5. PXRD patterns of **DMOF-1**.

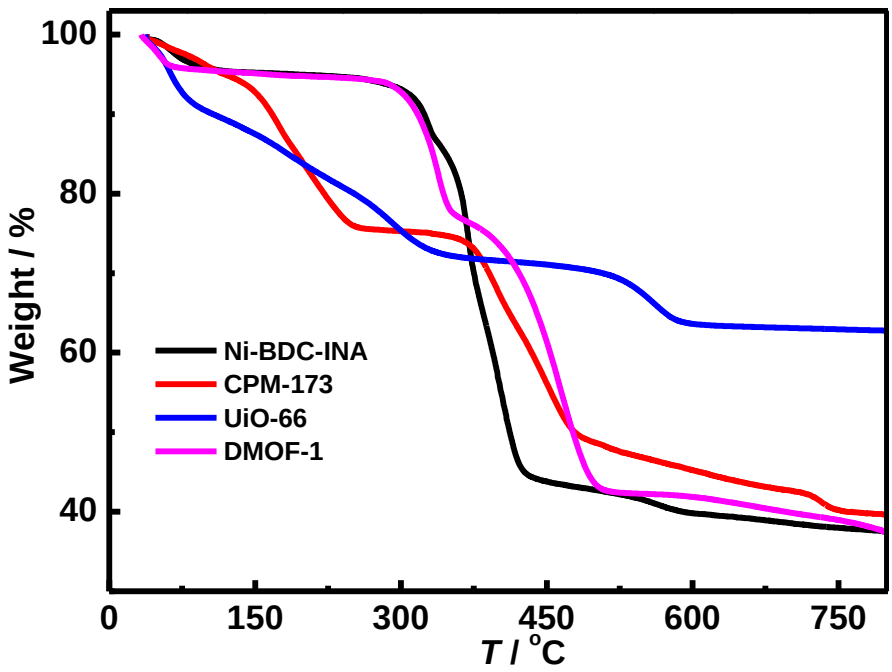

Figure S6. TG curves of **Ni-BDC-INA**, **CPM-173**, **UiO-66** and **DMOF-1**. (Note: all the as-synthesized samples were dried in air overnight before TG tests. We reason that the greater weight loss of **UiO-66** before 150 °C is mainly attributed to the volatile guest such as H_2O and DMF et al. Firstly during our synthesis, **Ni-BDC-INA** and **CPM-173** were synthesized using DMF and EtOH as mixed solvent and **UiO-66** was synthesized using DMF individually, the involved EtOH in **Ni-BDC-INA** and **CPM-173** would be more volatile during the air-dry progress, which makes **UiO-66** showed a greater weight loss. Secondly, there exist a lot of O^{2-}/OH^- donors around the Zr_6 clusters, which further afforded a hydrophilic pore environment for **UiO-66** and which make is possible to adsorb moisture to afford a greater weight loss compared with **DMOF-1**)

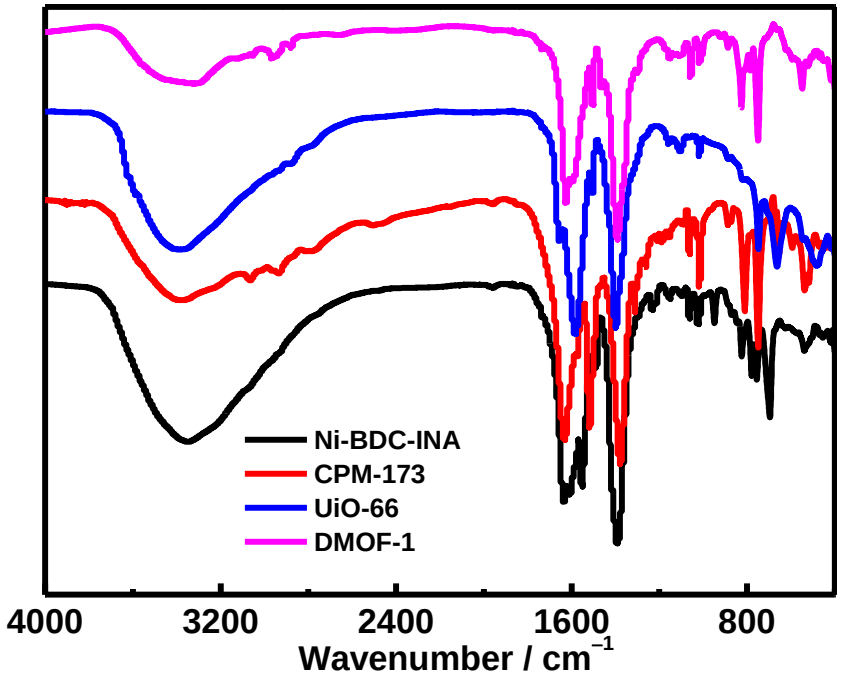

Figure S7. FT-IR spectra of **Ni-BDC-INA**, **CPM-173**, **UiO-66,** and **DMOF-1**.

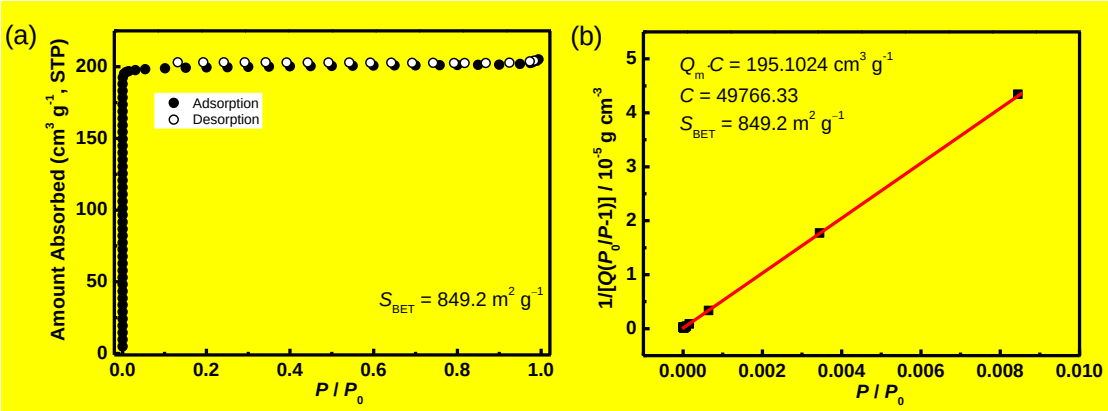

Figure S8. (a) N_2 adsorption isotherms at 77 K and (b) BET fitting of **Ni-BDC-INA.**

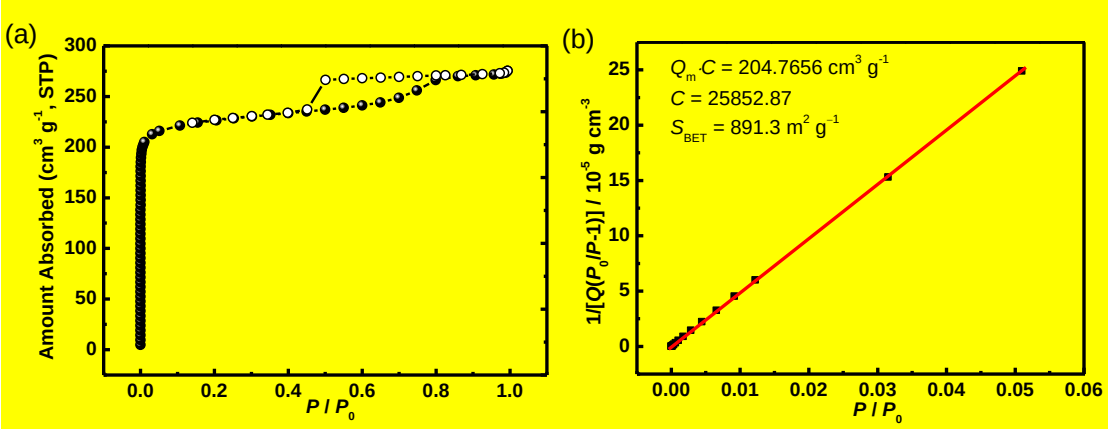

Figure S9. (a) N_2 adsorption isotherms at 77 K and (b) BET fitting of **CPM-173**.

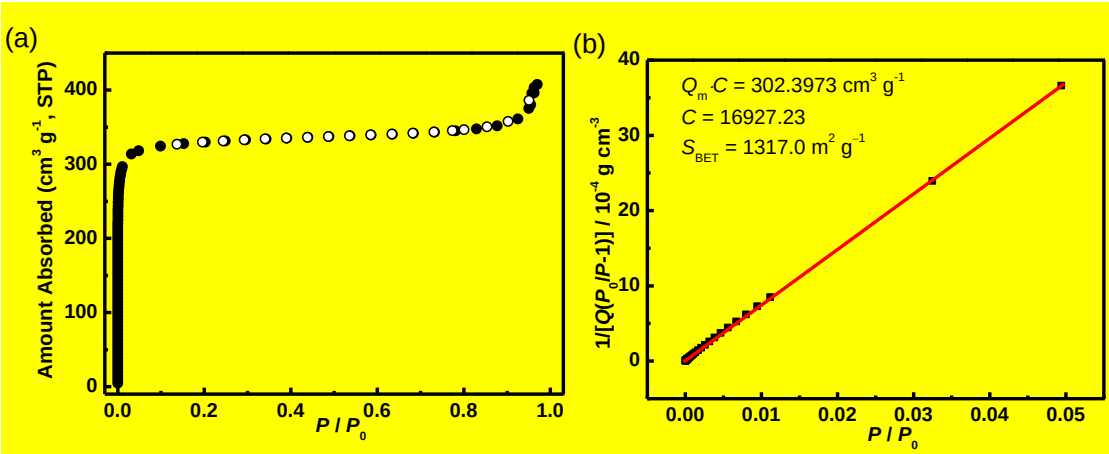

Figure S10. (a) N_2 adsorption isotherms at 77 K and (b) BET fitting of **UiO-66.**

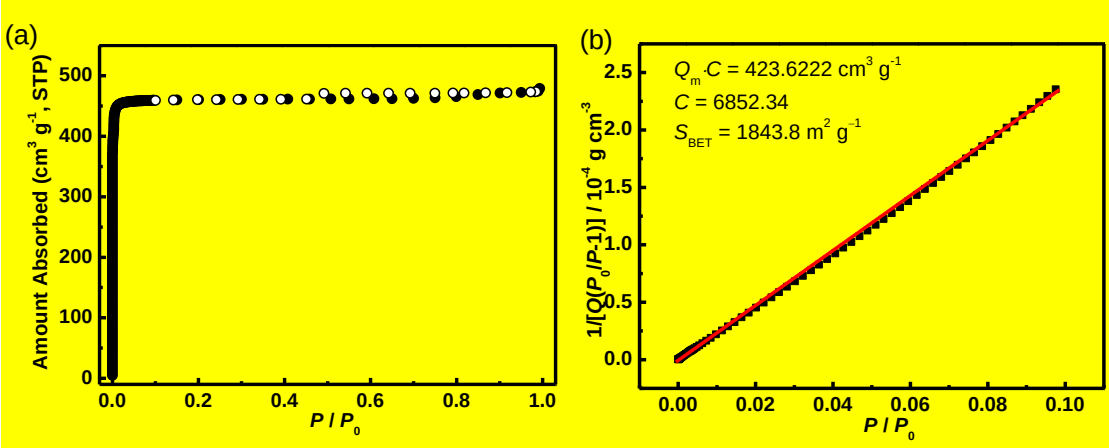

Figure S11. (a) N_2 adsorption isotherms at 77 K and (b) BET fitting of **DMOF-1.**

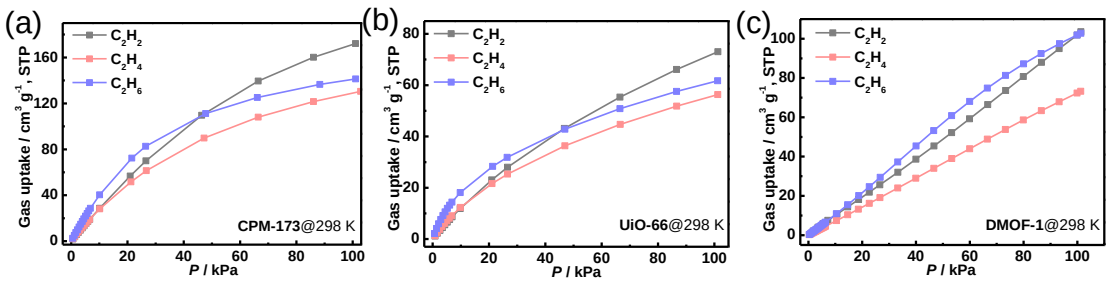

Figure S12. The C2 gases adsorption isotherms at 298 K for (a) **CPM-173,** (b) **UiO-66,** (c) **DMOF-1**.

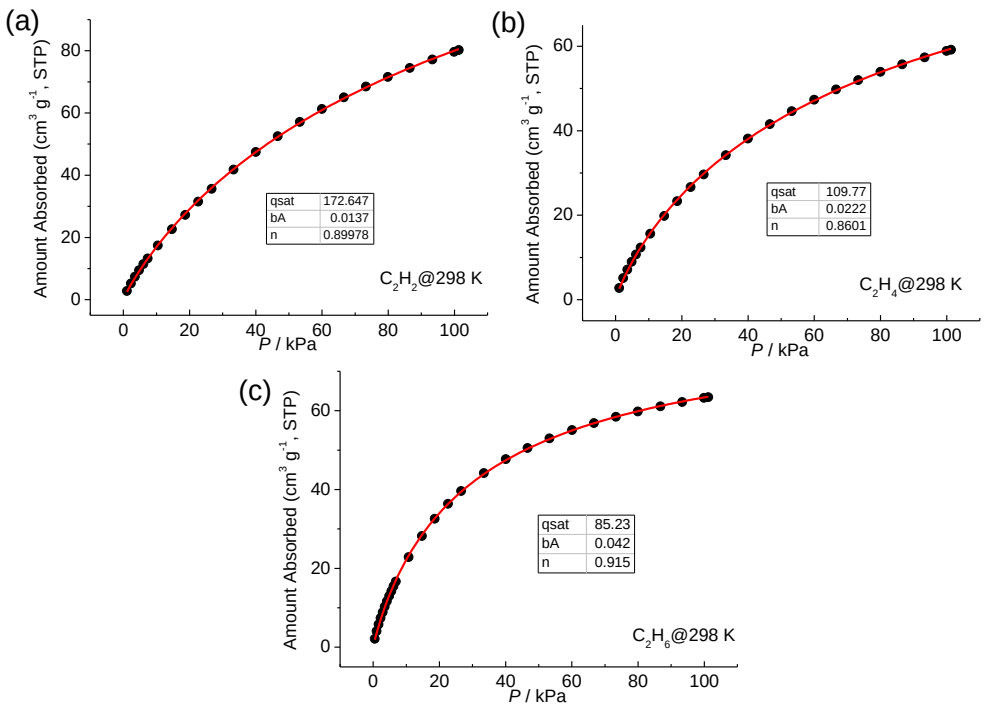

Figure S13. The Langmuir-Freundlich fitting details for **Ni-BDC-INA** and the solid lines are the best fit for the data.

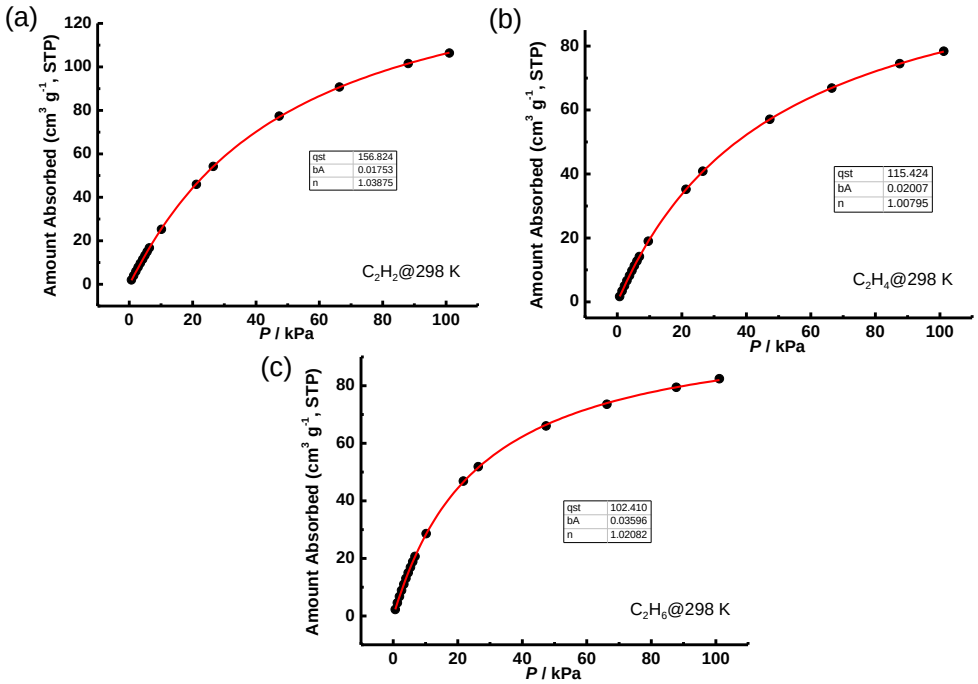

Figure S14. The Langmuir-Freundlich fitting details for **CPM-173** and the solid lines are the best fit for the data.

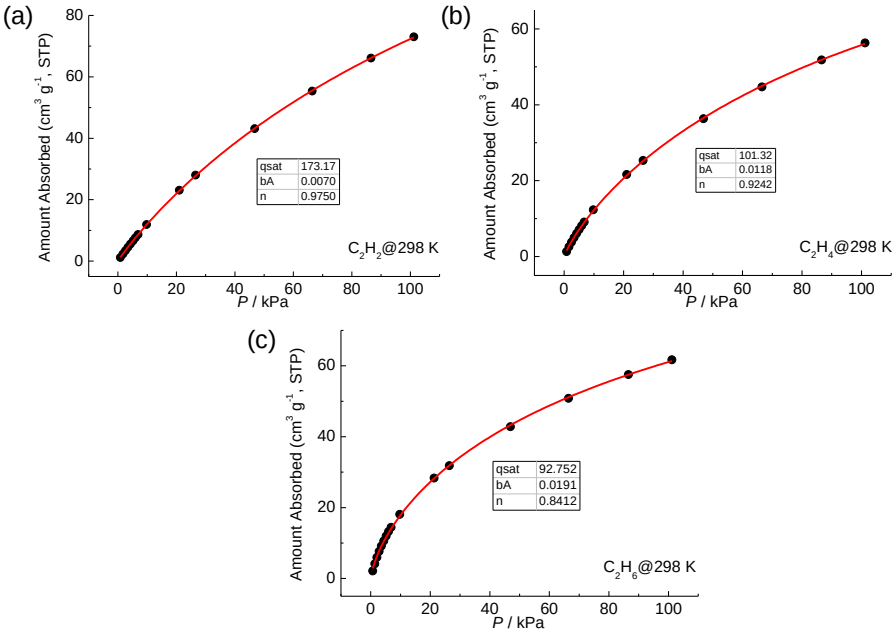

Figure S15. The Langmuir-Freundlich fitting details for **UiO-66** and the solid lines are the best fit for the data.

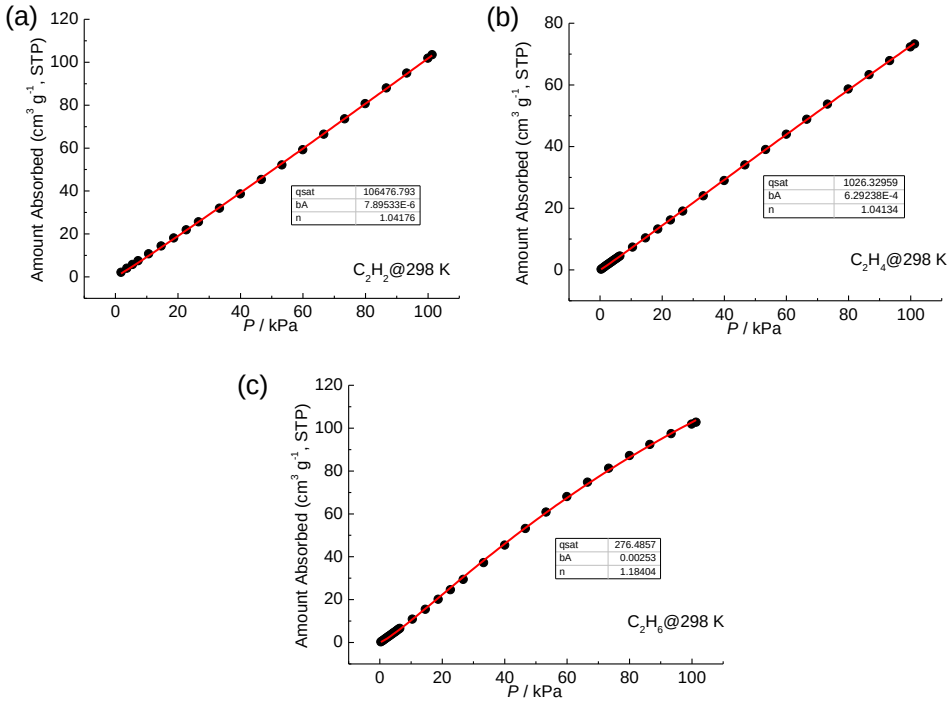

Figure S16. The Langmuir-Freundlich fitting details for **DMOF-1** and the solid lines are the best fit for the data.

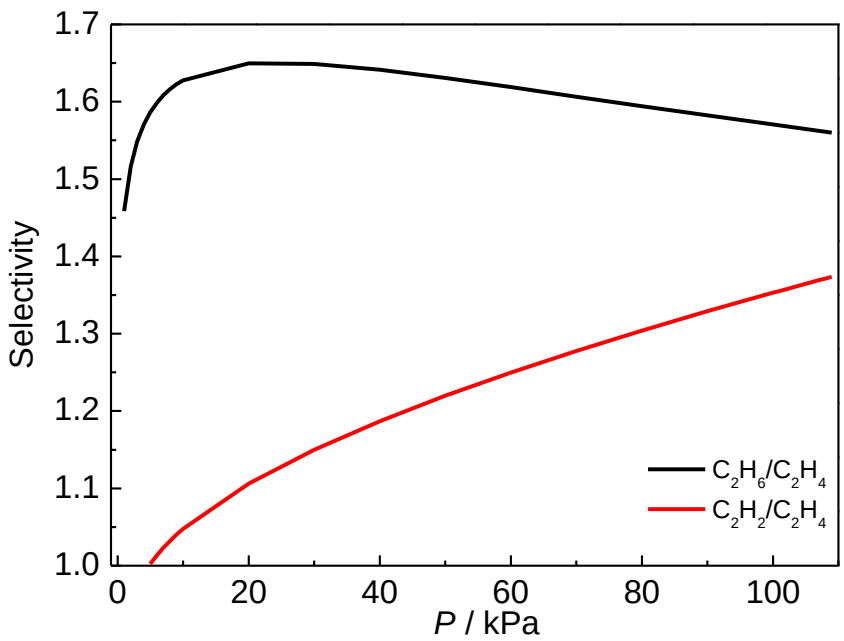

Figure S17. IAST selectivity of **Ni-BDC-INA** for 50:50 equimolar gas mixture at 298 K.

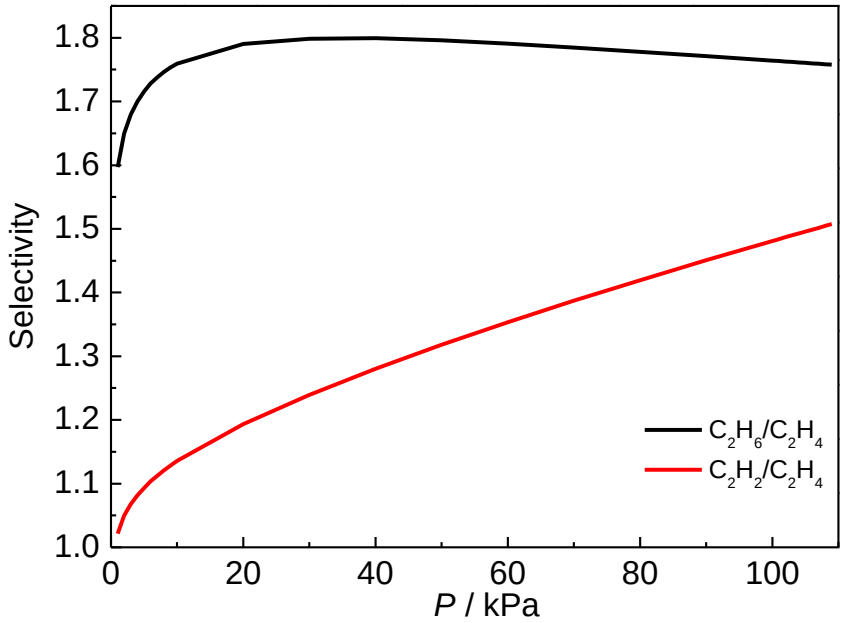

Figure S18. IAST selectivity of **CPM-173** for 50:50 equimolar gas mixture at 298 K.

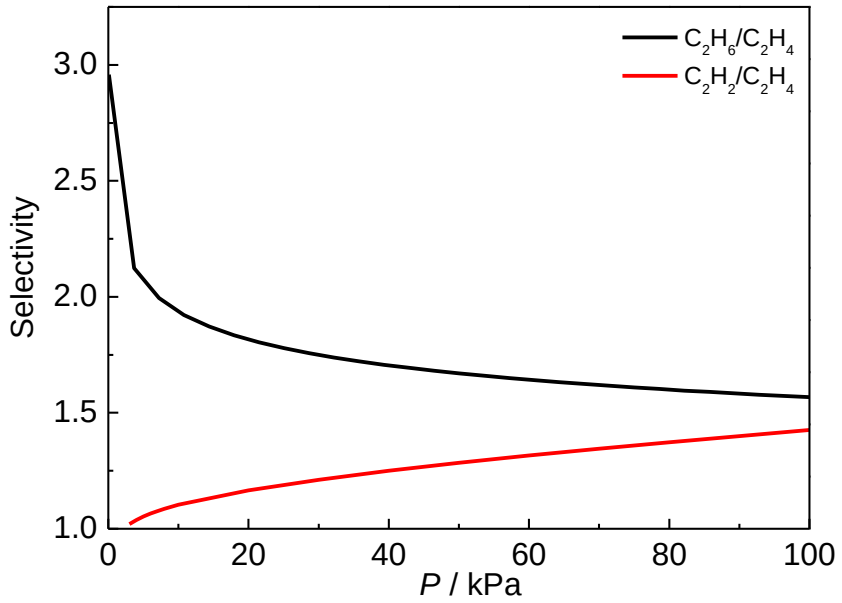

Figure S19. IAST selectivity of **UiO-66** for 50:50 equimolar gas mixture at 298 K.

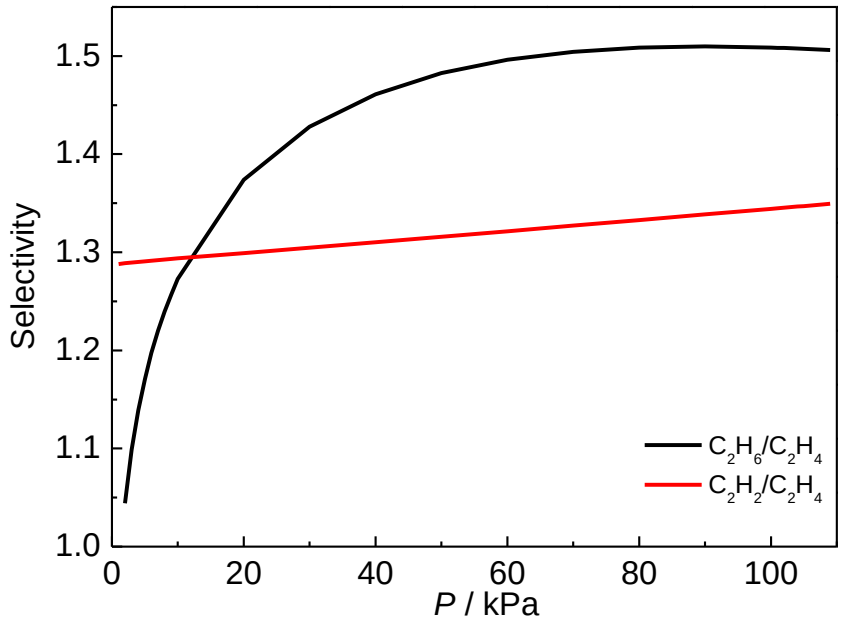

Figure S20. IAST selectivity of **DMOF-1** for 50:50 equimolar gas mixture at 298 K.

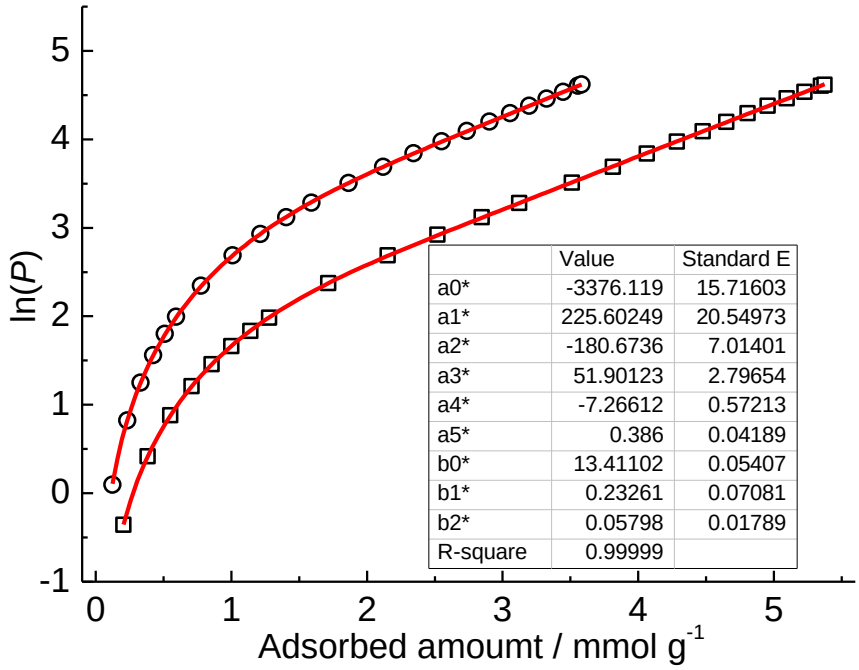

	Value	Standard E
a0*	-3376.119	15.71603
a1*	225.60249	20.54973
a2*	-180.6736	7.01401
a3*	51.90123	2.79654
a4*	-7.26612	0.57213
a5*	0.386	0.04189
b0*	13.41102	0.05407
b1*	0.23261	0.07081
b2*	0.05798	0.01789
R-square	0.99999	

Figure S21. The fitting details of C_2H_2 adsorption isothermals for **Ni-BDC-INA** using the virial method. Square; 273 K, circle, 298 K, and the solid lines are the best fit of the data.

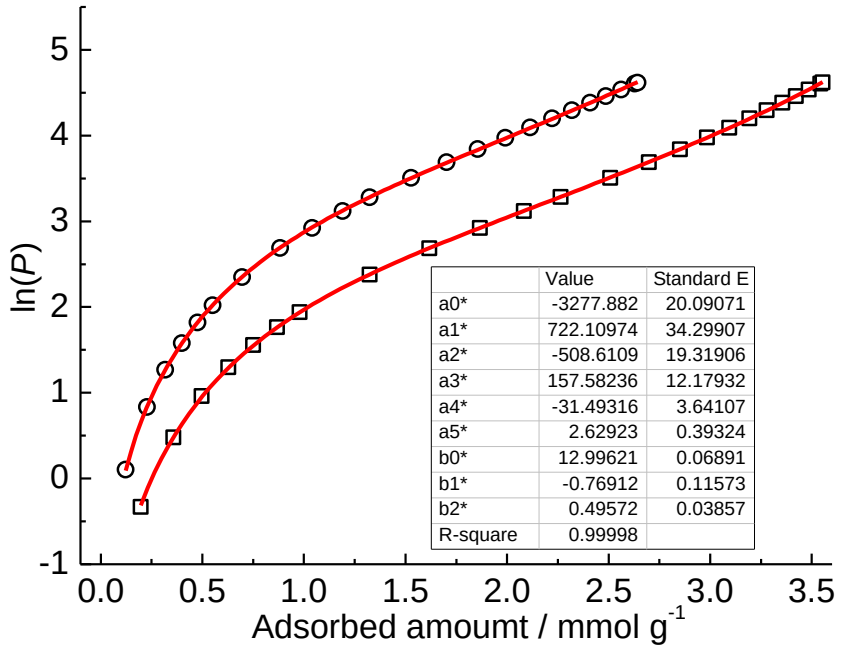

Figure S22. The fitting details of C_2H_4 adsorption isothermals for **Ni-BDC-INA** using the virial method. Square; 273 K, circle, 298 K, and the solid lines are the best fit of the data.

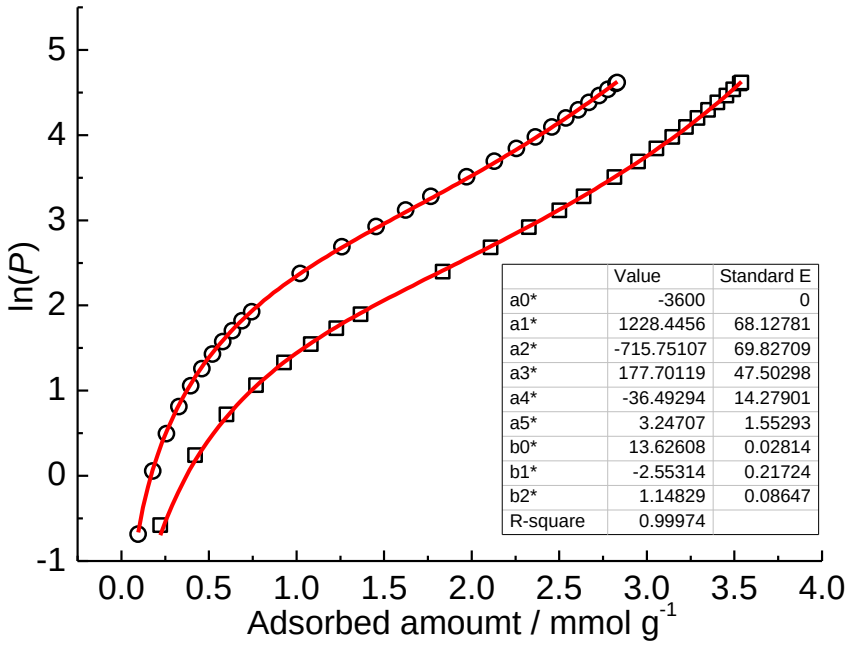

Figure S23. The fitting details of C_2H_6 adsorption isothermals for **Ni-BDC-INA** using the virial method. Square; 273 K, circle, 298 K, and the solid lines are the best fit of the data.

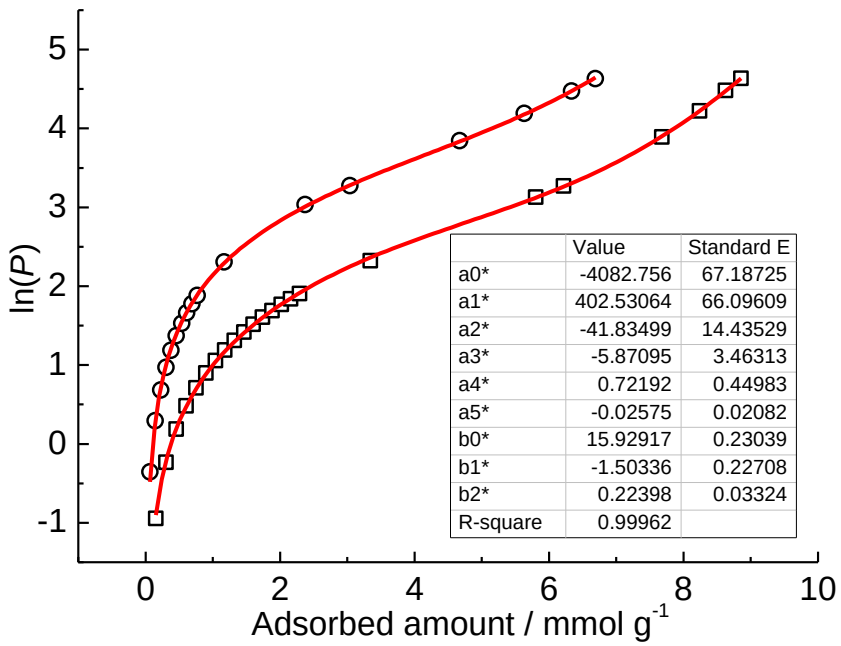

Figure S24. The fitting details of C_2H_2 adsorption isothermals for **CPM-173** using the virial method. Square; 273 K, circle, 298 K, and the solid lines are the best fit of the data.

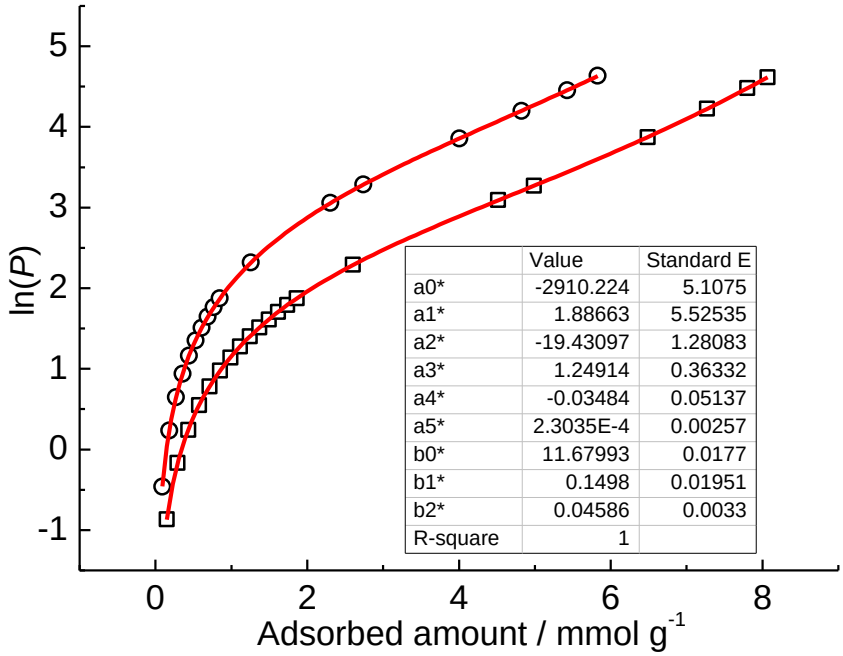

Figure S25. The fitting details of C_2H_4 adsorption isothermals for **CPM-173** using the virial method. Square; 273 K, circle, 298 K, and the solid lines are the best fit of the data.

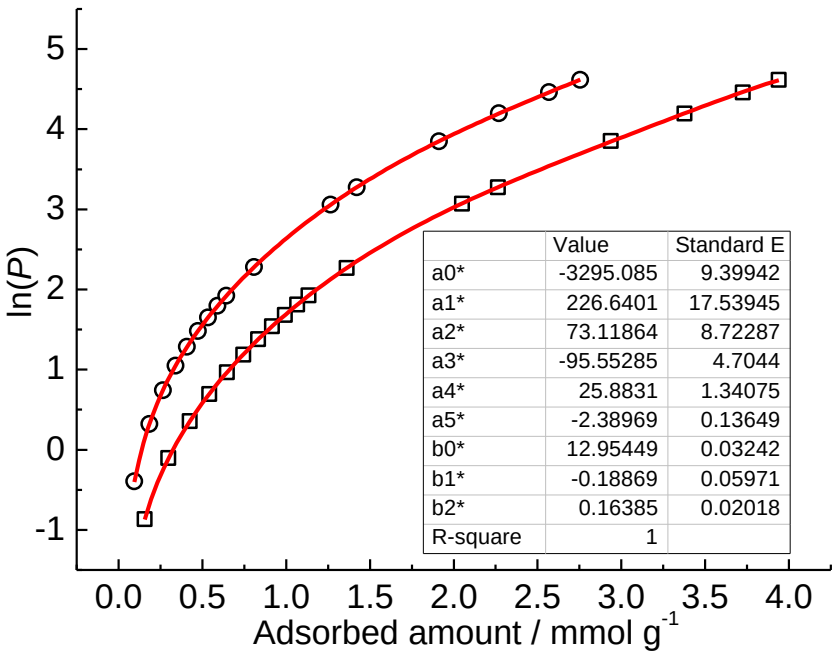

Figure S26. The fitting details of C_2H_6 adsorption isothermals for **CPM-173** using the virial method. Square; 273 K, circle, 298 K, and the solid lines are the best fit of the data.

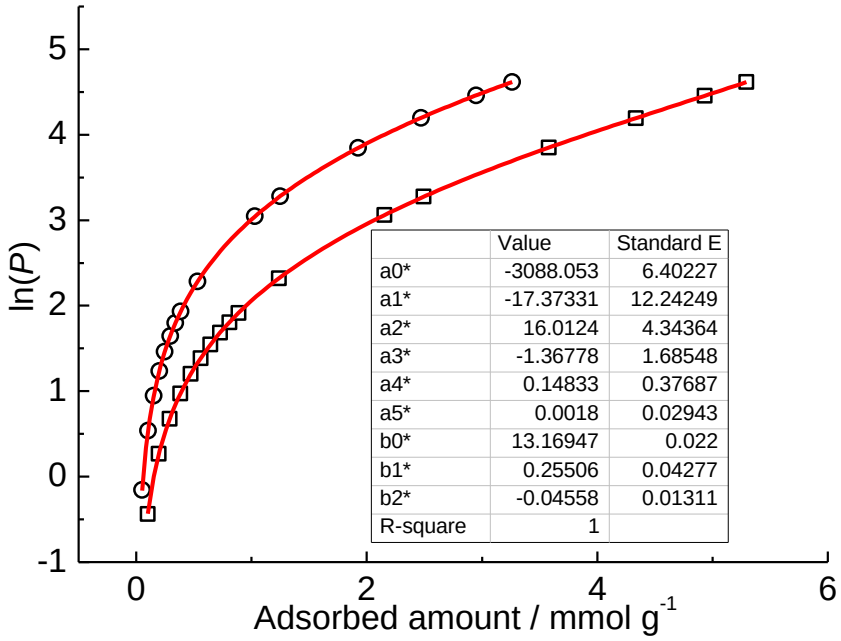

Figure S27. The fitting details of C_2H_2 adsorption isothermals for **UiO-66** using the virial method. Square; 273 K, circle, 298 K, and the solid lines are the best fit of the data.

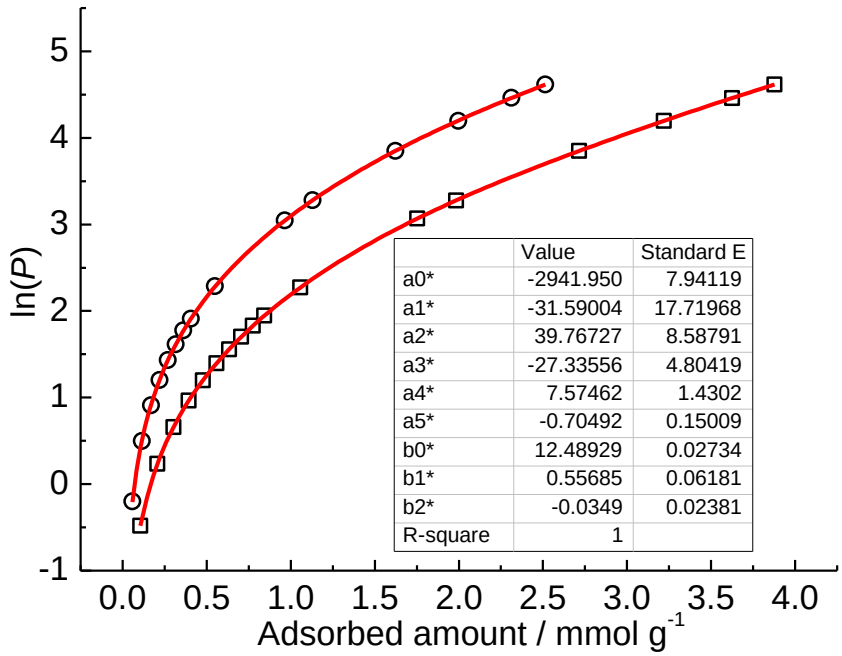

Figure S28. The fitting details of C_2H_4 adsorption isothermals for **UiO-66** using the virial method. Square; 273 K, circle, 298 K, and the solid lines are the best fit of the data.

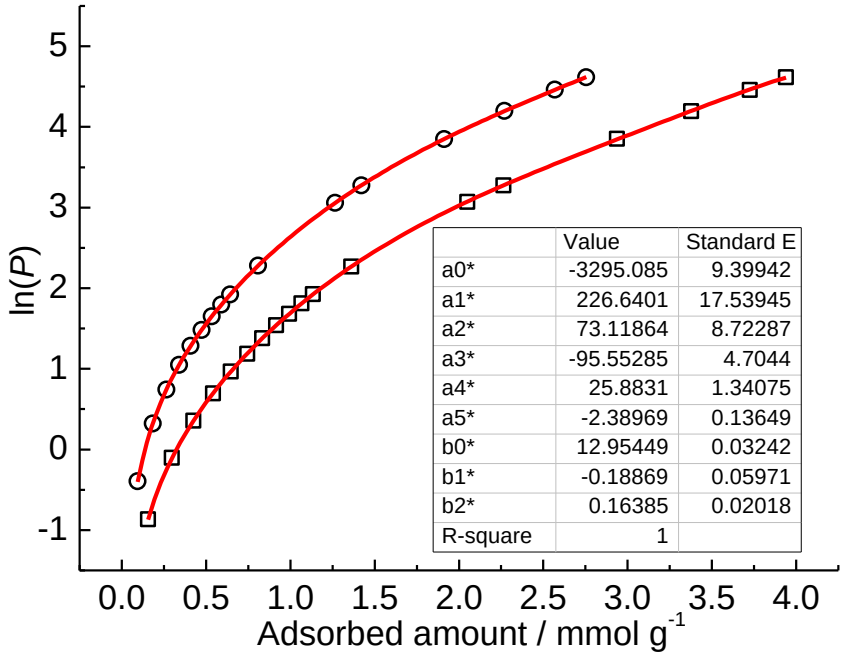

Figure S29. The fitting details of C_2H_6 adsorption isothermals for **UiO-66** using the virial method. Square; 273 K, circle, 298 K, and the solid lines are the best fit of the data.

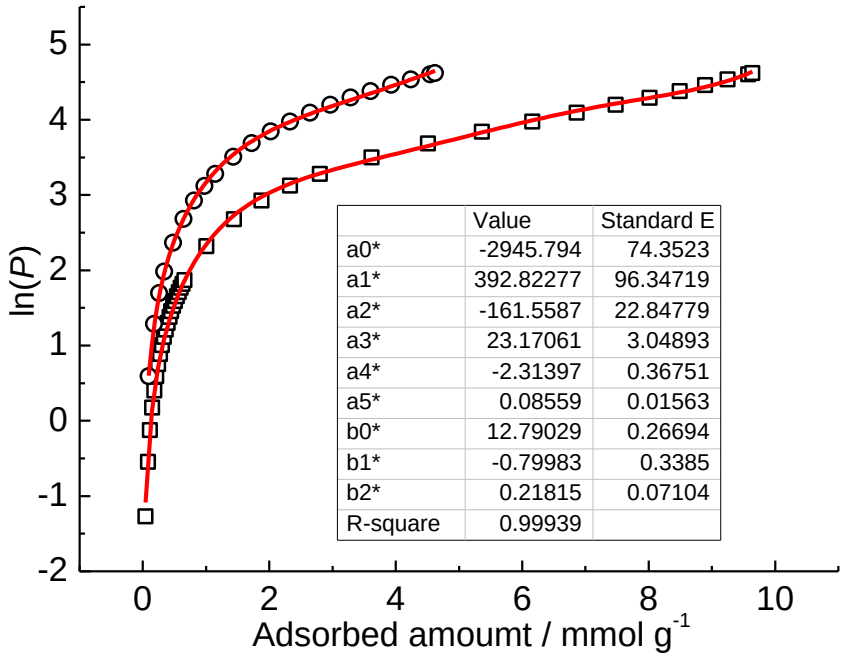

Figure S30. The fitting details of C_2H_2 adsorption isothermals for **DMOF-1** using the virial method. Square; 273 K, circle, 298 K, and the solid lines are the best fit of the data.

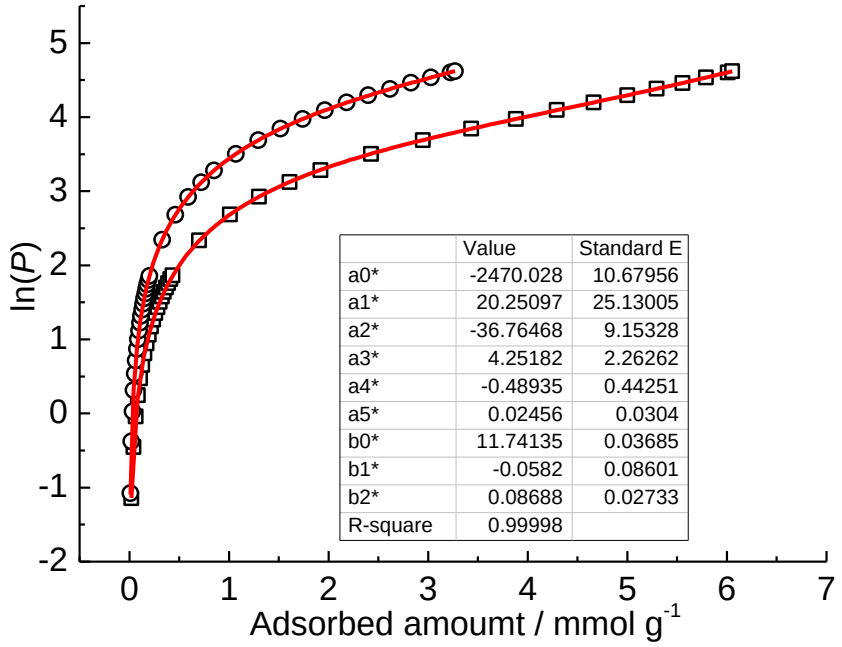

Figure S31. The fitting details of C_2H_4 adsorption isothermals for **DMOF-1** using the virial method. Square; 273 K, circle, 298 K, and the solid lines are the best fit of the data.

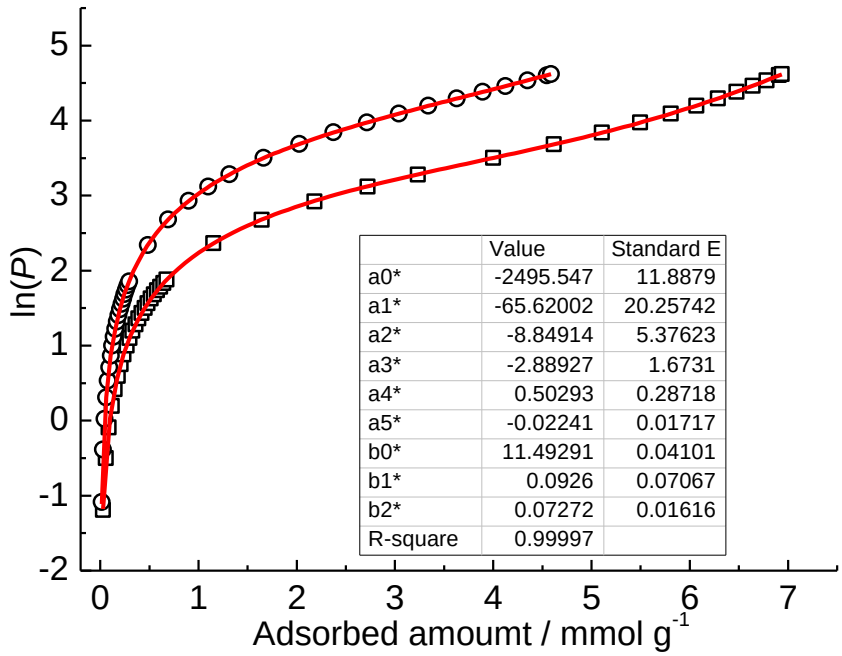

Figure S32. The fitting details of C_2H_6 adsorption isothermals for **DMOF-1** using the virial method. Square; 273 K, circle, 298 K, and the solid lines are the best fit of the data.

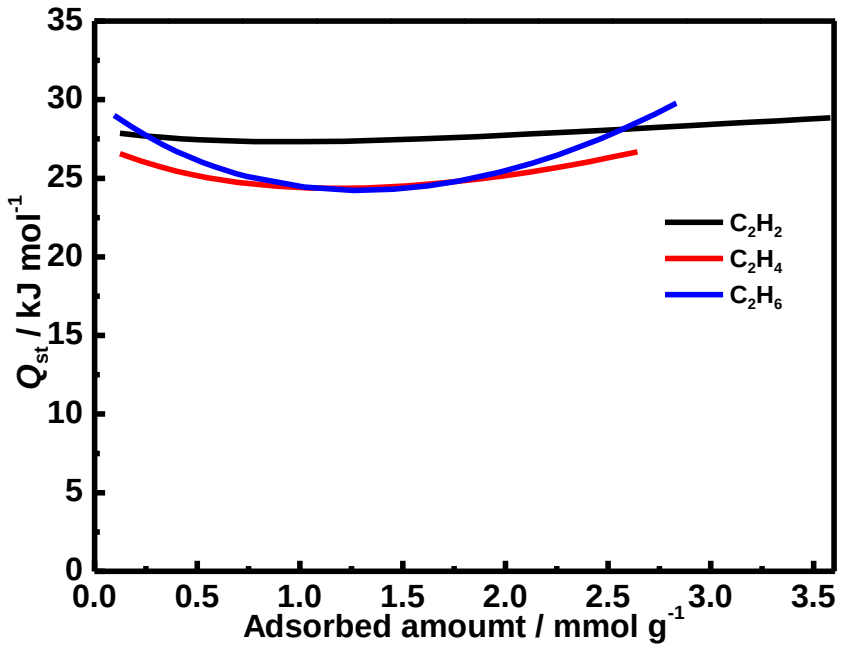

Figure S33. Calculated Q_{st} of **Ni-BDC-INA** for C2 gases.

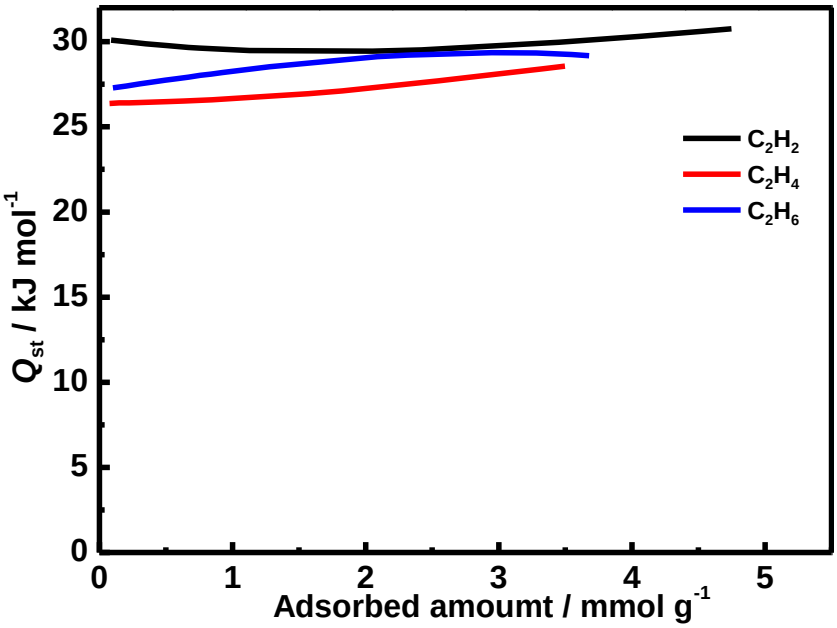

Figure S34. Calculated Q_{st} of **CPM-173** for C2 gases.

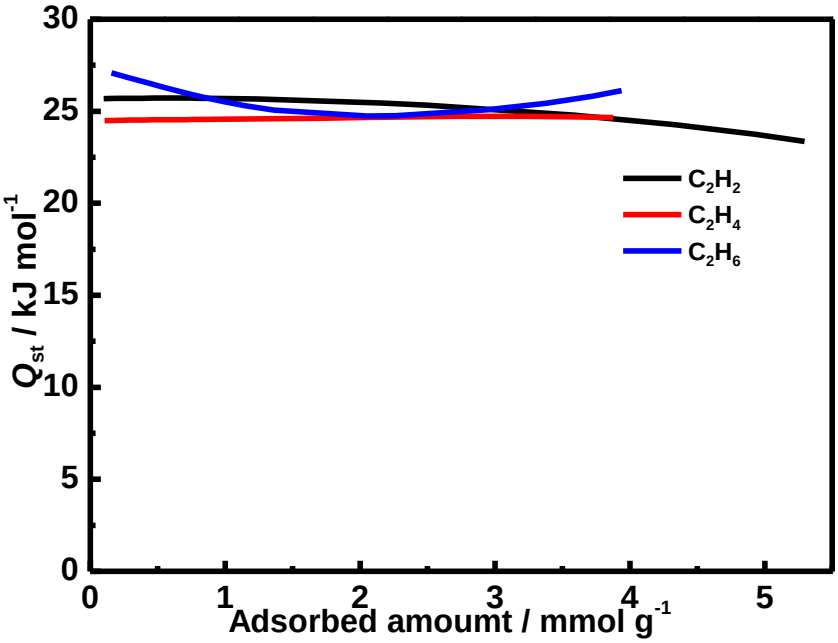

Figure S35. Calculated Q_{st} of **UiO-66** for C2 gases.

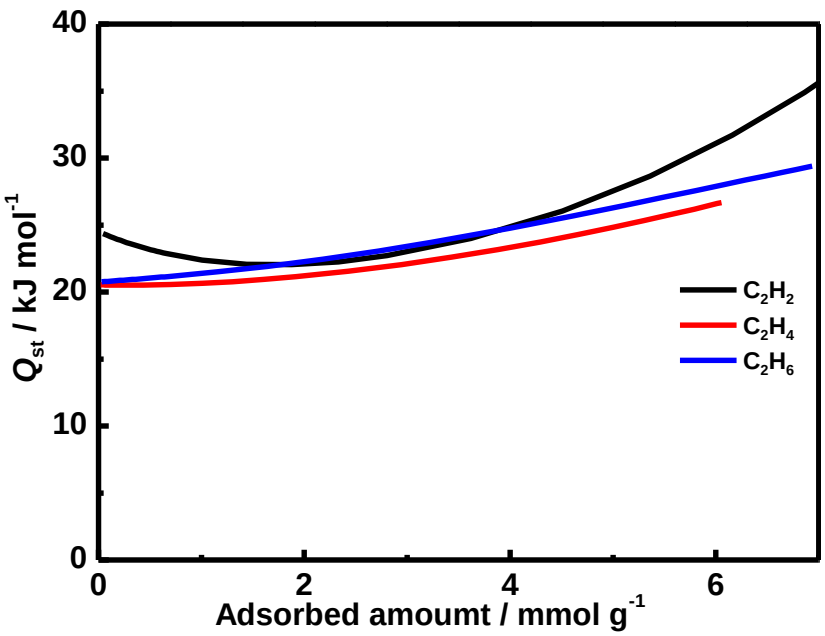

Figure S36. Calculated Q_{st} of **DMOF-1** for C2 gases.

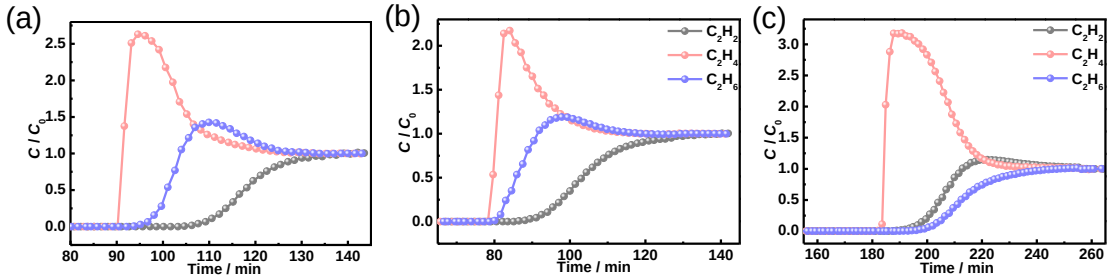

Figure S37. The breakthrough experiments at 298 K using 1:1:1 gas ternary with flow rate of 1.5 cm^3 min^{-1} (right) for (a) **CPM-173,** (b) **UiO-66** (c) **DMOF-1**.

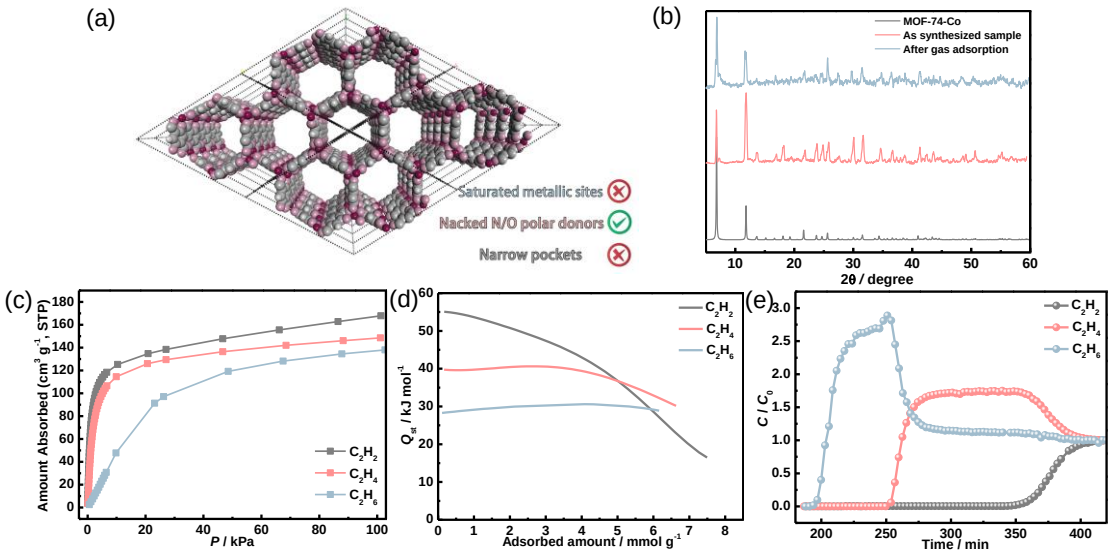

Figure S38. (a) The pore features for **MOF-74-Co**; (b) PXRD patterns for indicated samples; (c) C2 gases adsorption isotherms at 298 K; (d) Calculated Q_{st} of **MOF-74-Co** for C2 gases; (e) The breakthrough experiments at 298 K using 1:1:1 gas ternary with flow rate of 1.5 cm^3 min^{-1} for

MOF-74-Co.

We selected **MOF-74-Co** which is famous for the high density of open metal sites[6] as the first counterexample. The isotherm plots (Fig. S38c) showed strong adsorption behavior of unsaturated C_2H_2 and C_2H_4 over C_2H_6, which have been attributed to be the coordination effect between the open metal site and unsaturated bonds. And the gas uptakes reach up to 167.9 cm^3 g^{-1} for C_2H_2, 148.5 cm^3 g^{-1} for C_2H_4 and 138.0 cm^3 g^{-1} for C_2H_6 at 1 bar and 298 K. Furthermore, the adsorption enthalpies (Q_{st}) were calculated to be 55.06 kJ mol^{-1} for C_2H_2, 39.73 kJ mol^{-1} for C_2H_4 and 28.29 kJ mol^{-1} for C_2H_6, confirming the strong binding effect towards unsaturated C_2H_2 and C_2H_4. Finally, as shown in Fig. S38e, the multiple-component breakthrough experiment revealed the first breakthrough content of C_2H_6 followed by C_2H_4 and C_2H_2, in good agreement with the Q_{st} of C_2H_6 < C_2H_4 < C_2H_2. Taken together, all the observations are fully support our proposal for the pore features.

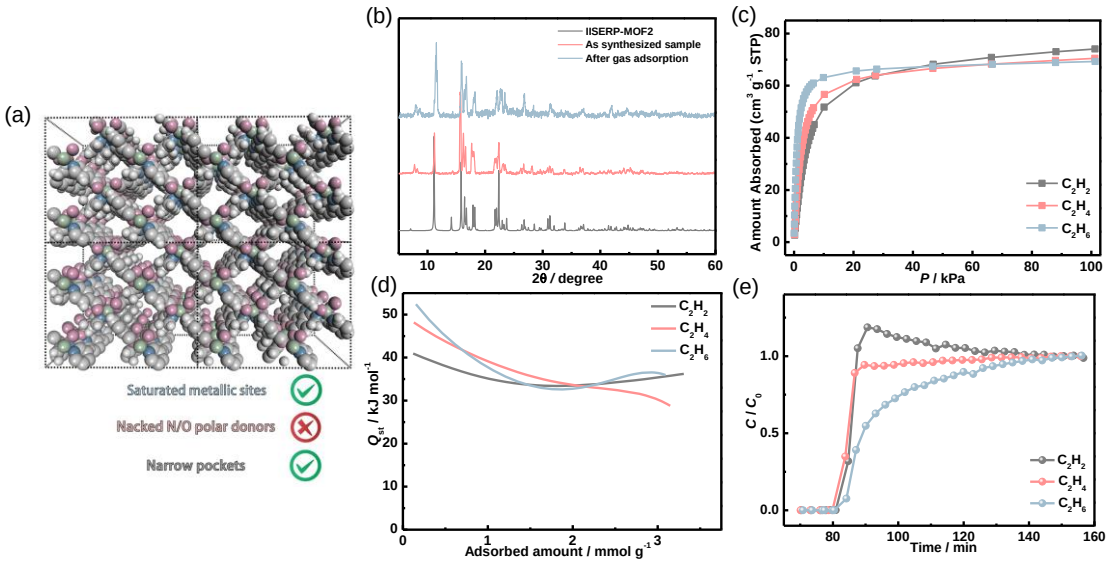

Figure S39. (a) The pore features for **IISERP-MOF2**; (b) PXRD patterns for indicated samples; (c) C2 gases adsorption isotherms at 298 K; (d) Calculated Q_{st} of **IISERP-MOF2** for C2 gases; (e) The breakthrough experiments at 298 K using 1:1:1 gas ternary with flow rate of 1.5 cm^3 min^{-1} for **IISERP-MOF2.**

IISERP-MOF2 was selected as the second counterexample. **IISERP-MOF2** exhibits narrow pockets for C_2H_6 capture which has been well studied by Hong et al[23] and our group[7]. However, the incomplete exposing of N/O donor atoms reduces the binding effect towards C_2H_2, which further makes the separation of C_2H_4 fail. The isotherm plots (Fig. S39c) showed strong adsorption behavior of C_2H_2, C_2H_4 and C_2H_6 owing to the fit-lake-a-glove manner of the narrow pocket and gas molecules. And the isotherm plots for all gases at 298 K exhibited Type-I behavior and gas uptakes reach up to 74.1 cm^3 g^{-1} for C_2H_2, 70.5 cm^3 g^{-1} for C_2H_4 and 69.3 cm^3 g^{-1} for C_2H_6 at 1 bar and 298 K. Furthermore, the adsorption enthalpies (Q_{st}) were calculated to be 40.93 kJ mol^{-1} for C_2H_2, 48.18 kJ mol^{-1} for C_2H_4 and 52.41 kJ mol^{-1} for C_2H_6, confirming the strong binding effect towards all C2 gases. Finally, although the breakthrough time of gas contents were just in line with the detection limit of our home-made facility, we can see the multiple-component

breakthrough experiment revealed the first breakthrough content of C_2H_2 and C_2H_4 followed by C_2H_6, which further confirm the proposal.

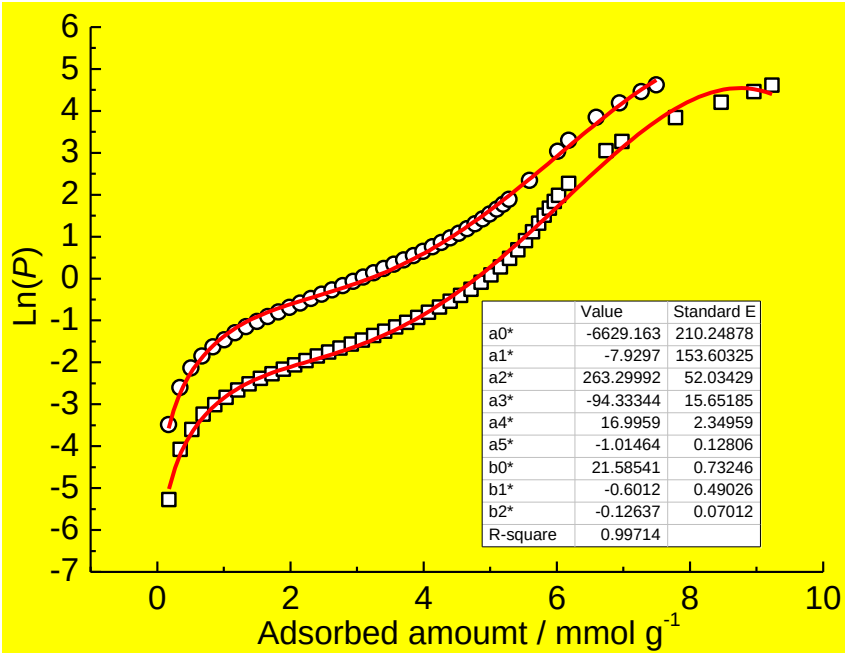

Figure S40. The fitting details of C_2H_2 adsorption isothermals for **MOF-74-Co** using the virial method. Square; 273 K, circle, 298 K, and the solid lines are the best fit of the data.

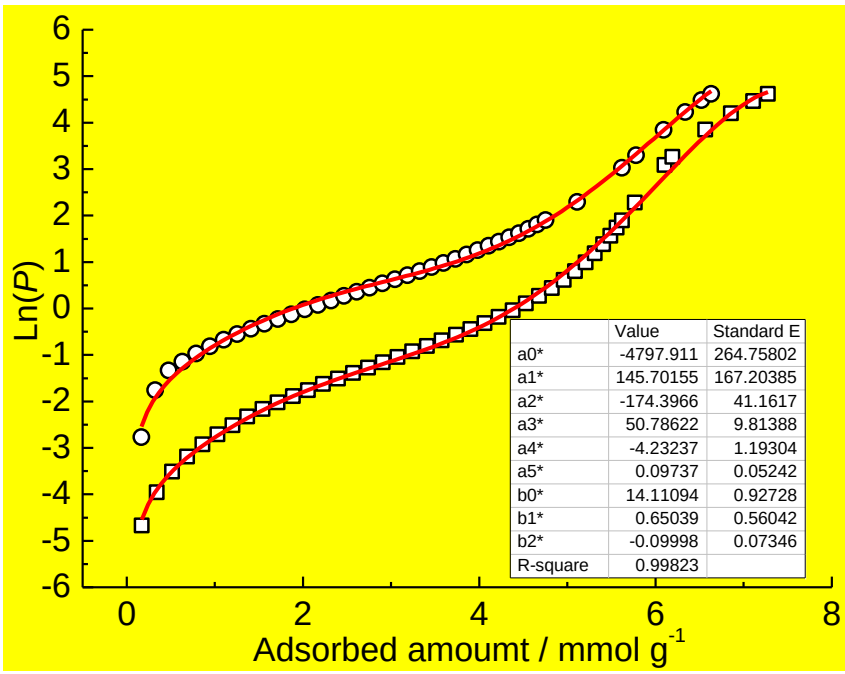

Figure S41. The fitting details of C_2H_4 adsorption isothermals for **MOF-74-Co** using the virial method. Square; 273 K, circle, 298 K, and the solid lines are the best fit of the data.

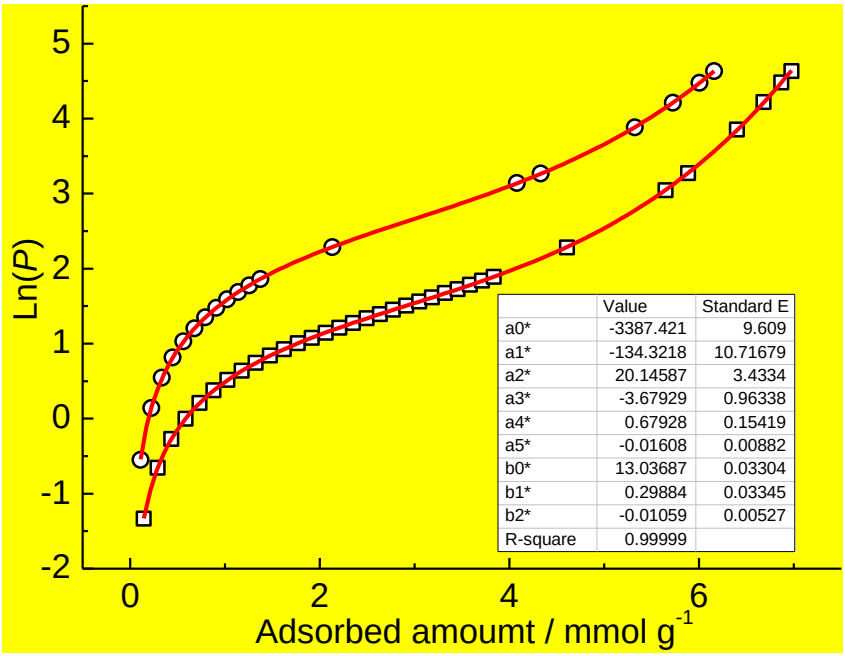

Figure S42. The fitting details of C_2H_6 adsorption isothermals for **MOF-74-Co** using the virial method. Square; 273 K, circle, 298 K, and the solid lines are the best fit of the data.

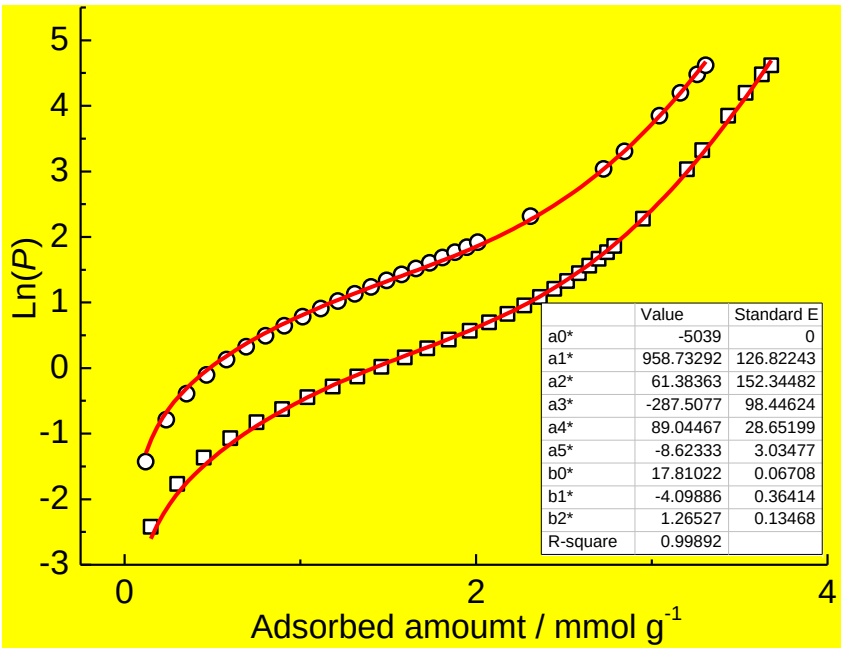

Figure S43. The fitting details of C_2H_2 adsorption isothermals for **IISERP-MOF2** using the virial method. Square; 273 K, circle, 298 K, and the solid lines are the best fit of the data.

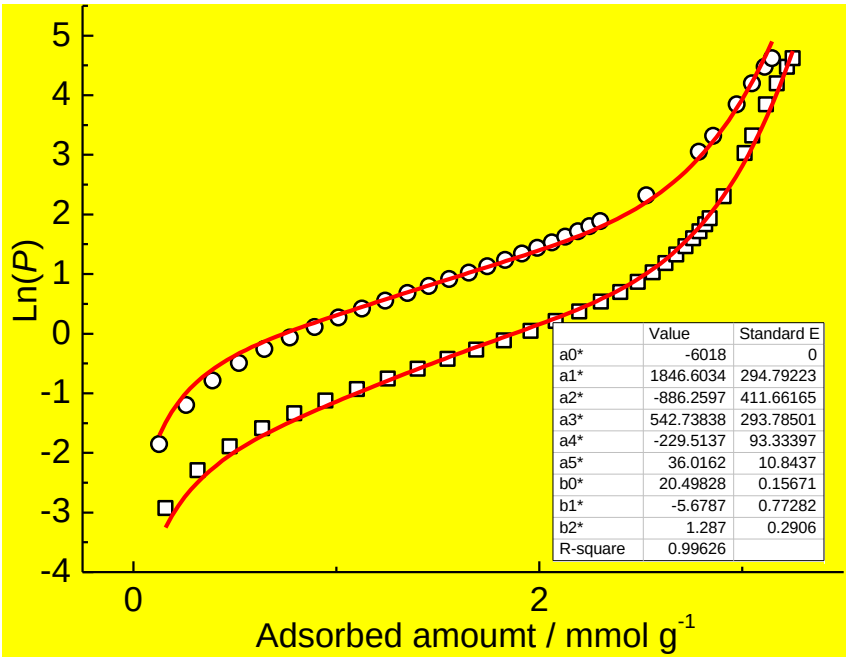

Figure S44. The fitting details of C_2H_4 adsorption isothermals for **IISERP-MOF2** using the virial method. Square; 273 K, circle, 298 K, and the solid lines are the best fit of the data.

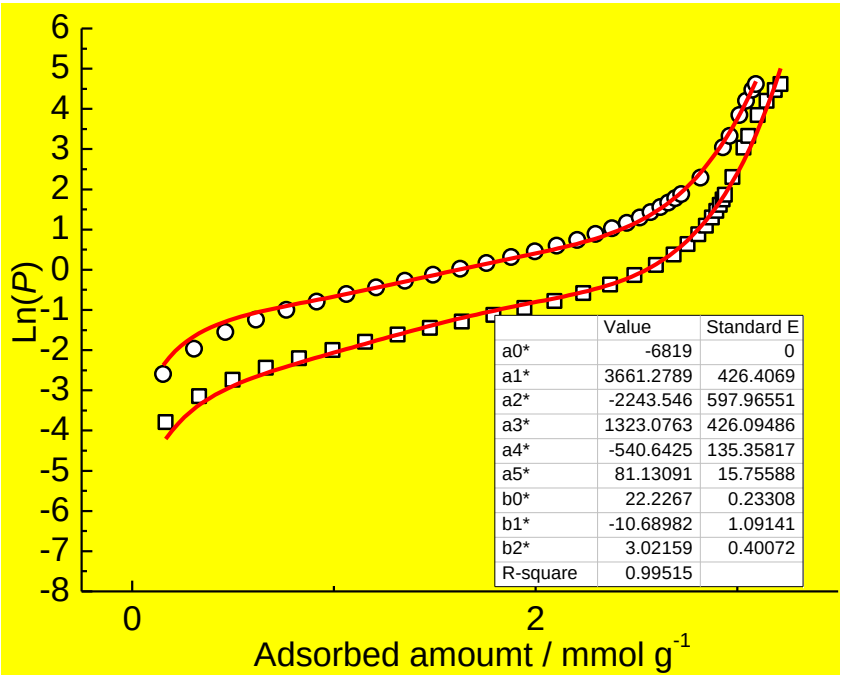

Figure S45. The fitting details of C_2H_6 adsorption isothermals for **IISERP-MOF2** using the virial method. Square; 273 K, circle, 298 K, and the solid lines are the best fit of the data.

References:

[1] M. Li, Z. Miao, M. Shao, S. Liang, S. Zhu, *Inorg. Chem.* 2008, **47**, 4481-4489.

[2] Y. Zhang, H. Zhou, R. Lin, C. Zhang, J. Lin, J. Zhang, X. Chen, *Nat. Commun.* 2012, **3**, 642.

[3] T. Zhang, Y. Hu, T. Han, Y. Zhai, Y. Zheng, *ACS Appl. Mater. Interfaces* 2018, **10**, 15786-15792.

[4] J. H. Cavka, S. Jakobsen, U. Olsbye, N. Guillou, C. Lamberti, S. Bordiga, K. P. Lillerud, *J. Am. Chem. Soc.* 2008**, 130**, 13850-13851.

[5] D. N. Dybtsev, H. Chun, K. Kim, *Angew. Chem. Int. Ed.* 2004, **43**, 5033-5036.

[6] S. Xiang, W. Zhou, Z. Zhang, M. A. Green, Y. Liu and B. Chen, *Angew. Chem. Int. Ed.*, 2010, **49**, 4615-4618.

[7] X. Jiang, Y. Wang, J. W. Cao, Z. M. Ye, T. Zhang, D. X. Liu, K. L. Li, R. Yang, T. Wang, Q. Y. Zhang and K. J. Chen, *Chem. Eur. J.* 2021, **27**, 12753-12757.

[8] S. Nandi, S. Collins, D. Chakraborty, D. Banerjee, P. K. Thallapally, T. K. Woo and R. Vaidhyanathan, *J. Am. Chem. Soc.* 2017, **139**, 1734-1737.

[9] A. L. Myers, J. M. Prausnitz, *AIChE J.* 1965, **11**, 121-127.

[10] B. Zhu, J. Cao, S. Mukherjee, T. Pham, T. Zhang, T. Wang, X. Jiang, K. A. Forrest, M. J. Zaworotko, K. Chen, *J. Am. Chem. Soc.* 2021, **143**, 1485-1492.

[11] H. G. Hao, Y. F. Zhao, D. M. Chen, J. M. Yu, K. Tan, S. Ma, Y. Chabal, Z. M. Zhang, J. M. Dou, Z. H. Xiao, G. Day, H. C. Zhou, T. B. Lu, *Angew. Chem. Int. Ed.* 2018, **57**, 16067-16071.

[12] Z. Xu, X. Xiong, J. Xiong, R. Krishna, L. Li, Y. Fan, F. Luo, B. Chen, *Nat. Commun.* 2020, **11**, 3163.

[13] L. Fan, P. Zhou, X. Wang, L. Yue, L. Li, Y. He, *Inorg. Chem.* 2021, **60**, 10819-10829.

[14] P. Liu, Y. Wang, Y. Chen, J. Yang, X. Wang, L. Li, J. Li, *Sep. Purif. Technol.* 2021, **276**, 119284.

[15] Y. Wang, C. Hao, W. Fan, M. Fu, X. Wang, Z. Wang, L. Zhu, Y. Li, X. Lu, F. Dai, Z. Kang, R. Wang, W. Guo, S. Hu, D. Sun, *Angew. Chem. Int. Ed.* 2021, **60**, 11350-11358.

[16] S. Yang, F. Sun, P. Liu, L. Li, R. Krishna, Y. Zhang, Q. Li, L. Zhou, T. Hu, *ACS Appl. Mater. Interfaces.* 2021, **13**, 962-969.

[17] J. Cao, S. Mukherjee, T. Pham, Y. Wang, T. Wang, T. Zhang, X. Jiang, H. Tang, K. A. Forrest, B. Space, M. J. Zaworotko and K. Chen, *Nat. Commun.* 2021, **12**, 6507.

[18] Z. Jiang, L. Fan, P. Zhou, T. Xu, S. Hu, J. Chen, D. Chen and Y. He, *Inorg. Chem. Front.*, 2021, **8**, 1243-1252.

[19] X. Gu, J. Wang, E. Wu, H. Wu, W. Zhou, G. Qian, B. Chen and B. Li, *J. Am Chem Soc*, 2022, **144**, 2614-2623.

[20] L. Czepirski, J. JagieŁŁo, *Chem. Eng. Sci.* 1989, **44**, 797-801.

[21] N. Metropolis, A. W. Rosenbluth, M. N. Rosenbluth, A. H. Teller, E. Teller, *J. Chem. Phys.* 1953, **21**, 1087-1092.

[22] A. K. Rappé, K. S. Colwell, C. J. Casewit, *Inorg. Chem.* 1993, **32**, 3438-3450.

[23] M. Kang, S. Yoon, S. Ga, D. W. Kang, S. Han, J. H. Choe, H. Kim, D. W. Kim, Y. G. Chung and C. S. Hong, *Adv. Sci.*, 2021, **8**, 2004940.